Kentucky Geological Survey
University of Kentucky, Lexington

Site Characteristics, Instrumentation, and Recordings of the Central United States Seismic Observatory

Edward W. Woolery, Zhenming Wang, and N. Seth Carpenter

Report of Investigations 37 Series XII, 2016

Our Mission

Our mission is to increase knowledge and understanding of the mineral, energy, and water resources, geologic hazards, and geology of Kentucky for the benefit of the Commonwealth and Nation.

Earth Resources—Our Common Wealth

www.uky.edu/kgs

Technical Level

General Intermediate Technical

ISSN 0075-5591

Contents

Figures

Figures
(Continued)

Site Characteristics, Instrumentation, and Recordings of the Central United States Seismic Observatory

Edward W. Woolery[1, 2], Zhenming Wang[2], and N. Seth Carpenter[2]

Abstract

The Central United States Seismic Observatory is a vertical seismic array in southwestern Kentucky within the New Madrid Seismic Zone. It is intended to record the effects of local geology, including thick sediment overburden, on seismic-wave propagation, particularly strong ground motion. The three-borehole array is composed of seismic sensors placed on the surface, in the bedrock, and at various depths within the 585-m-thick sediment overburden. The array's deep borehole also provides a unique opportunity to describe the geology and geophysically measure the complete Late Cretaceous through Quaternary stratigraphy in the northern Mississippi Embayment.

Based on surface and borehole geophysical measurements, the thick sediment overburden and its complex heterogeneous stratigraphy have been partitioned into a seven-layer sediment velocity model overlying a bedrock half-space. The S- and P-wave sediment velocities range between 160 and 875 m/s, and 1,000 and 2,300 m/s, respectively, and bedrock velocities between 1,452 and 3,775 m/s, respectively. In addition, high-resolution seismic-reflection profiles acquired within a 1-km radius of the array have imaged a complex geologic model, including steeply dipping N30°E-striking faults that have uplifted and arched post-Paleozoic sediments in a manner consistent with a dextral transpression component of displacement. The subparallel fault strands have been traced 1.4 km between reflection profiles and are adjacent to the array. The fault deformation extends above Paleozoic bedrock, affecting the Late Cretaceous and Eocene Mississippi Embayment sediments, as well as the base of the Quaternary. The Paleozoic and Cretaceous horizons show as much as 75 and 50 m of relief, respectively, with the middle Eocene and basal Quaternary disrupted 25 and 15 m, respectively. The differential fault offsets suggest episodic activity during the post-Paleozoic, and represent the first indications of Quaternary neotectonics in this part of Kentucky. More important, these faults may be the first evidence for a hypothesized northeast

[1]Department of Earth and Environmental Sciences, University of Kentucky
[2]Kentucky Geological Survey, University of Kentucky

extension of the strike-slip Axial Fault Zone from a through-going intersection with the left-stepover Reelfoot Fault (i.e., thrust).

Seismometers and accelerometers were both installed at the surface, 30 m, 259 m, and 526 m depths, and at 2 m into bedrock in three separate boreholes. The instrumentation elevation in the boreholes was determined by the major impedance boundaries within the stratigraphic section. Although the array operation has been frequently interrupted by the large hydrostatic pressures on the deeper instrumentation, the full array has recorded weak motions from 95 earthquakes at local, regional, and teleseismic distances. Initial observations reveal a complex spectral mix of amplification and deamplification across the array, indicating the site effect in this deep-sediment setting is not simply generated by the shallowest layers. Preliminary horizontal-to-vertical spectral ratio (HV) experiments show the bedrock vertical and horizontal amplitudes are not equal, violating a required assumption for site characterization. Furthermore, there are marked differences between spectral ratios from the directly measured transfer function (HH) and HV for particular earthquakes. On average, however, the HH and HV methods yield similar results within a narrow band of frequencies ranging between 0.35 and 1.1 Hz.

Introduction

The Central United States Seismic Observatory is a 21-component vertical seismic array located in southwestern Kentucky within the New Madrid Seismic Zone. This site is approximately 12 km northeast of the New Madrid Seismic Zone's most active area of seismicity, the central stepover thrust fault, and along the central axis of the thick sediment-filled Mississippi Embayment. The observatory is designed to evaluate the seismological engineering attributes associated with the regional seismic hazard, composed of three primary elements or effects: the earthquake source, path, and site effects. The observatory contributes to our understanding of each element, but is particularly well suited to better constrain the various field-based observational and theoretically based numerical approaches for defining the ground-motion site effect. Furthermore, it is among the deepest conventional continental-based vertical arrays in operation; thus, it offers both regional and global insight into the fundamental ground-motion behavior of deep-sediment environments.

There is broad scientific consensus that the thick sediment overburden of the northern Mississippi Embayment can produce ground-motion site effects from local earthquakes in the New Madrid Seismic Zone (Fig. 1). This is largely based on similar seismically active sediment-filled basins in other parts of the world that have shown that earthquake site effects can often produce detrimental societal consequences. In particular, observations from Mexico City during the Sept. 19, 1985, Michoacan earthquake (Seed and others, 1988) and the San Francisco Marina District during the Loma Prieta earthquake of Oct. 18, 1989 (Bonilla, 1991), clearly demonstrated that the local geology, including thick sediment overburden, significantly altered the amplitude, frequency content, and duration of earthquake ground motions. The extent of the ground-motion variation is determined by the local transfer function, which is defined by the dynamic properties and geometry of the local geology. The specific parameters include media elasticity, impedance contrasts within the sediment overburden and at the sediment–bedrock interface, sediment thickness, surface topography, sediment–bedrock interface geometry (i.e., horizontal, irregular, dipping, etc.), ground-motion amplitude (i.e., linear versus nonlinear), and the existence of lateral or vertical velocity gradients in the sediment or bedrock. Therefore, the resultant overall earthquake ground motion at any location is the result of the complex combination of source, path, and site effects, including 3D effects (see, for example, Bard and Chavez-Garcia, 1993; Anderson and others, 1996).

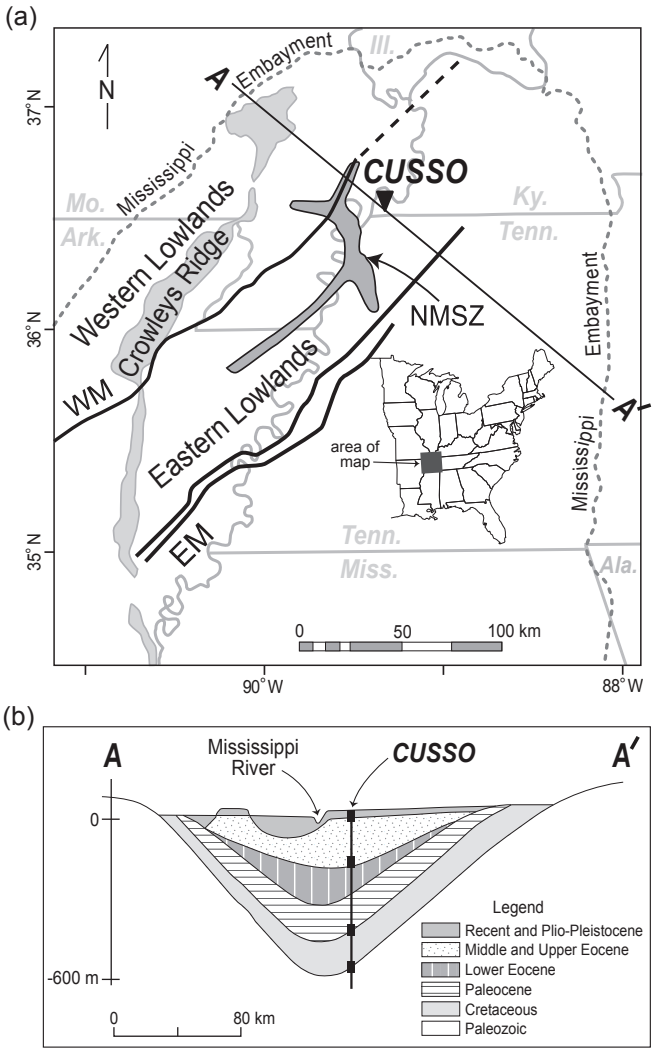

Figure 1. (a) Seismotectonic and physiographic setting of the study area. CUSSO is located approximately 12 km northeast of the northwest-oriented central stepover arm of the New Madrid Seismic Zone (dark gray shaded area). The seismic zone is located primarily in the Reelfoot Rift (heavy black lines; EM = eastern margin; WM = western margin). Modified from Csontos and Van Arsdale (2008); used with permission of the Geological Society of America. The structure of the Reelfoot Rift area is overlain by the Mississippi Embayment sediments. (b) Cross section A–A' shows the relative location of CUSSO within the sediment overburden and central embayment axis.

Simplified-empirical, pseudo-theoretical, reference-site, and vertical-array methods are field-based measures often used for characterizing site effects; however, there is considerable uncertainty associated with each because they cannot constrain the complex causality, particularly in regions with deep basins containing thick heterogeneous sediment deposits (more than 100 m), such as the central United States (Steidl and others, 1996; Bommer and Abrahamson, 2006). The same complexity also prevents a theoretical numerical-based approach from providing an absolute rendering of the ground-motion response.

Consider first the simplified-empirical method for characterizing the site effect. This approach has two requisite parameters: the incoming bedrock ground motion and time-weighted average shear-wave velocity for the top 30 m (V_{S30}) of earth material (Building Seismic Safety Council, 2009). Generally, the site coefficient increases with decreasing V_{S30}. Seismic hazard maps for the United States have been developed by the U.S. Geological Survey and National Earthquake Hazard Reduction Program, and the site coefficient as defined by V_{S30} has been incorporated into the "NEHRP Recommended Provisions for Seismic Regulations for New Buildings and Other Structures" for more than 25 yr (Building Seismic Safety Council, 2009). The simplified procedure uses scaling factors and attempts to adjust the ground motions for a particular site's soil conditions. The scaling factors are defined for five site classes, A through E (site class F requires a site-specific evaluation), and are a function of the intensity of input ground motions. The site classes, however, are established only on the time-averaged shear-wave velocity of the top 30 m of soil or rock. Thus, the procedure assumes that only the top 30 m of soil significantly influences the ground motions at a site, which is a critical assumption, particularly when the soil is several hundred meters thick as in the New Madrid Seismic Zone. Anderson and others (1996) showed that damping properties of soils deeper than 30 m are as critical to the resulting free-surface ground motions as the shear-wave velocities of the upper 30 m of soil. Bard and Chavez-Garcia (1993) showed that the deeper layers of surficial sediments in Mexico City had a significant effect on the ground motions at the surface during the Michoacan earthquake in 1985; however, Molnar and others (2004) concluded that site response based on V_{S30} in the greater Victoria, British Columbia, area is in agreement with the intensities observed for the 2001 Nisqually earthquake in Washington state. Wald and Mori (2000) found that the simplified empirical characterizations based on V_{S30} approximated the site-response observations in the Los Angeles area, but the scat-

ter was large and inadequate to predict site amplification. Castellaro and others (2008) further stated site amplification is too complex to be characterized simply by V_{S30}, and using only time-averaged shear-wave velocities of the upper 30 m ignores the natural period(s) of the entire site, where the majority of amplification may occur.

As an alternative, the horizontal-to-vertical spectral ratio is a widely used, cost-effective method for estimating the site effect (Nakamura, 1989). This pseudo-theoretical observational approach can include using the horizontal-to-vertical spectral ratio of ambient-noise/microtremor (see, for example, Bodin and Horton, 1999; Castellaro and Mulargia, 2009), or the horizontal-to-vertical spectral ratio of the energetic part of earthquake S-waves (see, for example, Lermo and Chavez-Garcia, 1993; Castro and others, 1997; Chen and Atkinson, 2002). Both approaches assume that the vertical component of the ground motion is relatively uninfluenced by the geologic site conditions and that the effects of Rayleigh waves on the horizontal and vertical components are equivalent; thus, the resultant horizontal-to-vertical spectral ratio ideally removes the source and path effects of the noise, leaving only the site response signal (Castro and others, 1997; Bonnefoy-Claudet and others, 2006).

Another method frequently used for understanding the ground-motion response is a theoretical evaluation of either the one-, two-, or three-dimensional transfer function. The predictive 1D analytical approach (e.g., SHAKE, DEEPSOIL) is the current state-of-the-practice in earthquake engineering design. In this context, the most widely used algorithm to analyze the seismic response of soil deposits is SHAKE (Schnabel and others, 1972; Idriss and Sun, 1992). SHAKE uses equivalent-linear soil properties to model soil nonlinearity. In an equivalent-linear analysis, the shear modulus and damping ratio of each soil layer are varied as a function of the induced shear strain. Iterations are performed until the shear strains calculated by the program are compatible with the soil properties chosen to be representative for the site. The equivalent-linear procedure is most accurate for smaller-intensity ground motions in which nonlinearity is less pronounced, and for stiff soil deposits in which large strain is not induced even by large-intensity motions. For larger-intensity motions or softer soils, a fully nonlinear dynamic analysis is more appropriate. The nonlinear analysis models the shear stress-strain hysteresis loops exhibited by soils in laboratory tests, thereby changing the stiffness of the soil as earthquake shaking progresses. Consequently, nonlinear analysis more accurately describes the stress–strain response of the soil, including the ability to capture the long-period response of deep soil sites such as those found in the Mississippi Embayment. Nevertheless, comparisons between nonlinear and equivalent-linear computer programs indicate that both analytical procedures produce similar results for lower-intensity motions, in which nonlinearity is less pronounced. An interesting result of large shaking is smaller ground-motion prediction at the surface due to soil nonlinearity, a phenomenon widely observed in recorded strong ground motions (see, for example, Rong and others, 2016). Nevertheless, neither equivalent-linear nor nonlinear analyses have been adequately validated for soil depths greater than about 100 m.

The most direct and reliable way to separate an earthquake's source and path effects from the site effect is to simultaneously record the earthquake on bedrock and the ground surface. This can be performed in two ways: comparing free-field ground motions at one or more locations with a reference recording from a nearby rock site (Steidl and others, 1996), or using a vertical array of downhole (i.e., bedrock) and surface instruments (Archuleta and others, 1992; Field and others, 1998) and recording ground motions at a site simultaneously. To use the latter direct method for providing deep sedimentary site-effect characterization (i.e., strong- and weak-motion amplification and attenuation of seismically induced ground motions, including frequency and duration modulation) and a calibration for other regional free-field strong-motion network installations in the northern Mississippi Embayment of the central United States, as well as to better constrain the simplified-empirical, pseudo-theoretical, and theoretical-numerical approaches, the three-borehole, 21-component vertical seismic array, CUSSO, was installed near the most active part of the New Madrid Seismic Zone (Figs. 1 and 2). The deepest borehole penetrates 585 m of unlithified Mississippi Embayment sedi-

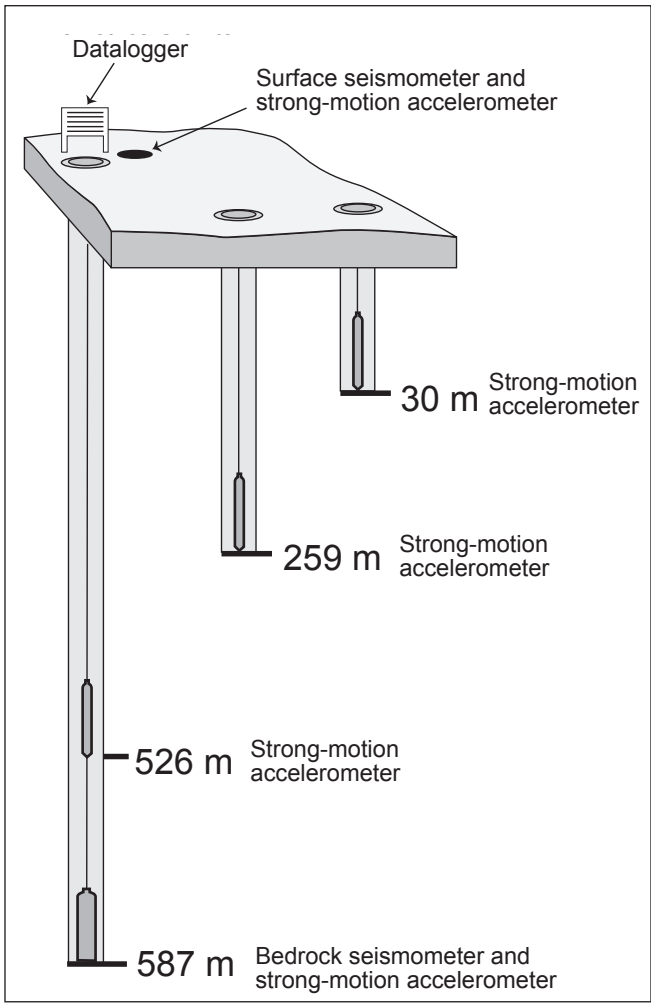

Figure 2. Schematic representation of the three-borehole CUSSO array, including the instrumentation and depth below ground surface. The 595-m-deep well is 23.5 and 25.5 m from the 259-m- and 30-m-deep wells, respectively. The 259-m- and 30-m-deep wells are 7.1 m apart. The free-surface instrumentation is offset from the 595-m-deep wellhead by 3.5 m.

ment and into the underlying bedrock, making it among the deepest conventional continental-based vertical seismic arrays in operation.

Site Characteristics

Geographically, CUSSO is located near the active seismicity associated with the New Madrid Seismic Zone in a small rural community situated within the Mississippi River floodplain of westernmost Kentucky (Fig. 1). The site coordinates are N36.5523°, W89.3297°, and the location is typical of what Toro and others (1992) referred to as embayment lowlands (i.e., floodplains) covering much of the northern Mississippi Embayment region of western Kentucky, southeastern Missouri, northwestern Tennessee, and northeastern Arkansas. Three important parts of the CUSSO location criteria are (1) proximity to an area of high seismicity in order to maximize the number of recorded events in the shortest amount of time, (2) site conditions typical of those found throughout the region and at most free-field regional seismic network stations, and (3) a long-term property right-of-entry. In other words, the location allows the observatory to act as a reference and calibration site for network stations throughout the embayment, and the land-use agreement provides longstanding deployment for recording the largest number of events of various magnitudes at the near, intermediate, and far fields.

The New Madrid Seismic Zone is an intraplate area of relatively high seismic-energy release, and includes a historic sequence of at least three large earthquakes (greater than M7) that occurred during the winter of 1811-12, as well as similar clustered events found in the paleoseismic record (Johnston and Schweig, 1996; Tuttle and others, 2002) (Fig. 1). These historic and paleoseismic events make the New Madrid Seismic Zone a primary contributor to the seismic hazard for much of the central United States. Most of the contemporary seismicity has been instrumentally located within the early Paleozoic Reelfoot Rift System and beneath the Late Cretaceous and early Tertiary Mississippi Embayment, an elongate southwest-plunging, sediment-filled basin that merges with the Gulf of Mexico coastal plain (Van Arsdale and TenBrink, 2000; Cox and Van Arsdale, 2002; Csontos and Van Arsdale, 2008). The earthquake epicenter patterns and associated focal solutions allow the complex seismic zone to be generalized as two northeast-oriented, dextral strike-slip fault zone segments offset by a central northwest-oriented, left-stepping restraining-bend thrust. CUSSO is located 12 km northeast of the most seismically active part of the zone, the central stepover, and near the central axis of the Mississippi Embayment (Fig. 1).

Site Stratigraphy

General. The Paleozoic bedrock was reached in the deepest of CUSSO's three boreholes, at 585 m be-

low ground surface. A relatively detailed description of the numerous unlithified post-Paleozoic sediment deposits is provided below, because there are few places in the northern Mississippi Embayment where the stratigraphic sequence for this overburden can be directly observed. Although retrieving in situ cored sediment samples was cost prohibitive, we were able to establish stratigraphic boundaries from both visual analysis of collected wellhead cuttings (Jonathan McIntyre and Steve Martin, Kentucky Geological Survey, 2009, personal communication) and a suite of downhole petrophysical logs by GeoVision Inc. (natural gamma, resistivity, and P/S sonic velocity) (Figs. 3–4). Cuttings generally represent a mixture of the sediment the drill bit passes through at certain depths, including from higher in the borehole; therefore cuttings cannot be used to describe intraformational features such as bedding or the nature of the formation contacts. Nevertheless, in the absence of core, they provide useful information on standard rock/sediment type and mineralogy at depth, which can be compared to geophysical logs in order to interpret subsurface stratigraphy.

Quaternary Alluvium (Pleistocene–Recent). The alluvium cover in the CUSSO borehole is 48 m thick and consists mostly of fine to coarse, variably colored sands. There is a substantial regional unconformity between Quaternary alluvium and underlying sediments in the region (Olive, 1980; McDowell and others, 1981). The contact between Quaternary sediments and the underlying Jackson Formation is interpreted in the CUSSO hole to be at the base of coarse sands and gravel; this is also indicated by a significant change in the natural gamma curve at 48 m (Fig. 3). Finch (1971) also indicated that gravel typically occurs at the base of the alluvium and at the base of older continental deposits above the Jackson Formation in the area.

Jackson Formation (and Possibly Upper Claiborne?) (Oligocene?–Eocene). The Jackson Formation in the region is an unlithified silty clay with a few interbedded silts and sands (Finch, 1971; Olive, 1980). Unfortunately, Jackson clays, silts, and sands are similar to the underlying Claiborne Formation, making visual distinction difficult. Davis and others (1973) could not differentiate the Jackson from underlying upper Claiborne in the

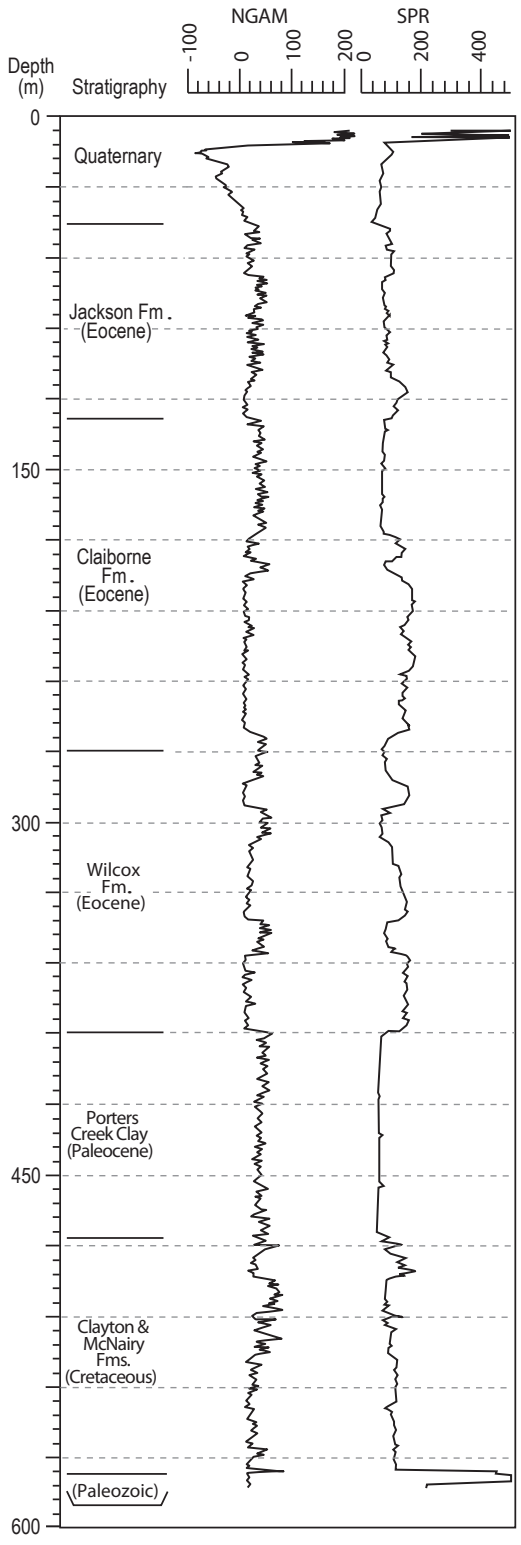

Figure 3. The CUSSO site consists of 585 m of unlithified sediment overlying the carbonate Paleozoic bedrock. The stratigraphic interpretation of the sediment was derived from the logged borehole cuttings during the drilling process, as well as natural-gamma and electrical-resistivity logs in the completed hole.

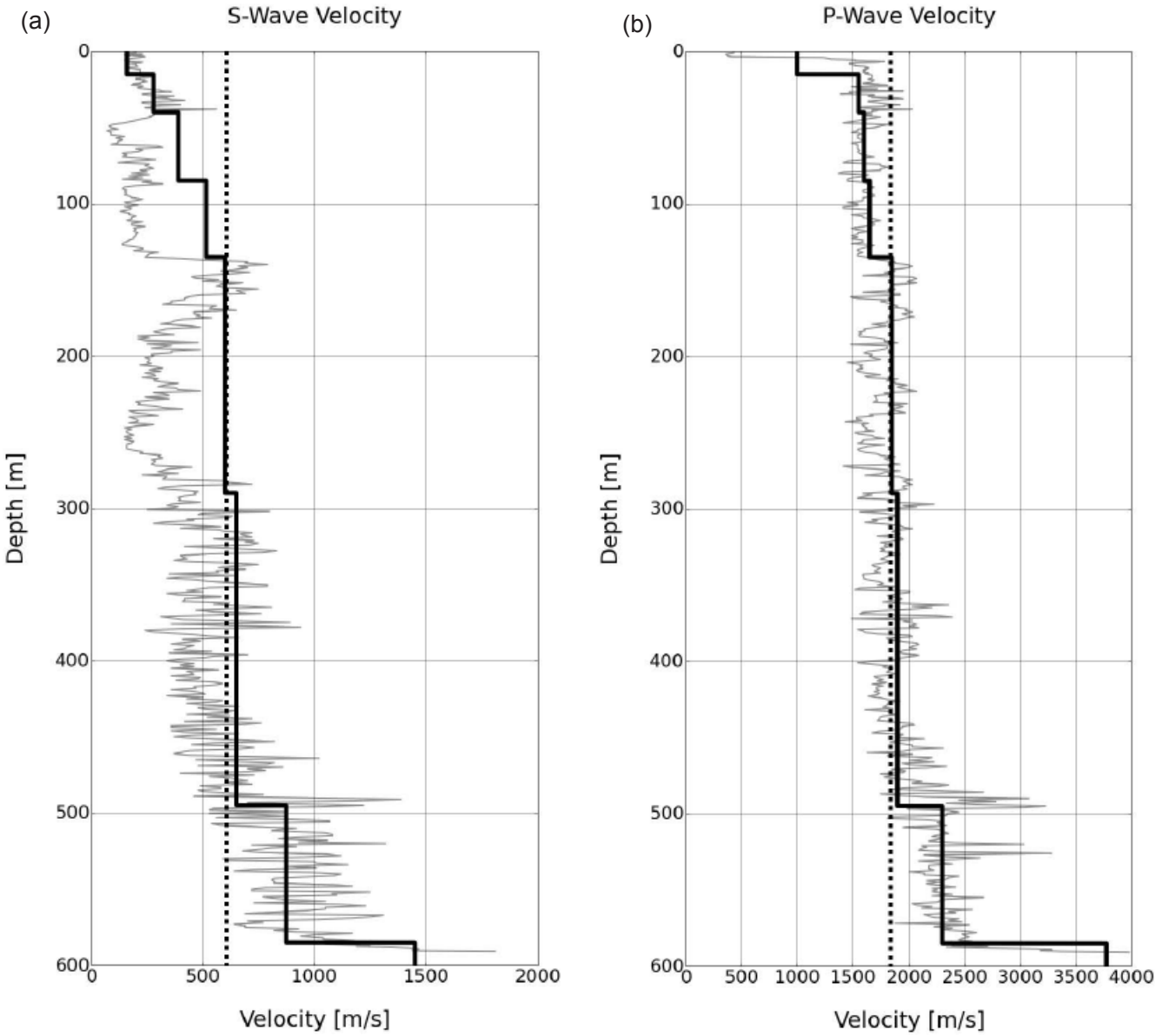

Figure 4. (a) Defined S-wave and (b) P-wave velocity models (solid black lines) for CUSSO. Compare these models with the S- and P-wave suspension-velocity logs (solid gray lines) and the average sediment velocity as measured by the phase arrival times across the instrumented array (vertical broken black lines). Two zones of anomalously low velocity occur in intervals 50–130 m and 180–265 m in both the P- and S-wave suspension logs, but are more pronounced in the S-wave log. We interpret the anomalies as artifacts of the drilling process in the immediate vicinity of the borehole. There was considerable borehole wall instability and collapse during drilling of these intervals; consequently, we speculate that the substantial sediment disturbance in the borehole annulus and immediate vicinity altered the velocity suspension log measurements.

nearby Florence No. 1 well, and correlated the combined Jackson through upper Claiborne interval as a single, undifferentiated unit. In the CUSSO well, the top of the Jackson Formation is placed at the base of a gravel and top of a black clay. The base of the unit is placed at the base of a sand overlying a sandy clay at 131 m; the unit also exhibited a distinct change in gamma-ray and resistivity-log response (Fig. 3). Davis and others (1973) placed the base of the Jackson–upper Claiborne interval at a level that could be correlated to the base of the Jackson as picked in the CUSSO well or possibly to a clay higher in the hole.

Claiborne Group (Lower–Middle Eocene). The contact between the Jackson and Claiborne Formations is regionally conformable (Olive, 1980). The Claiborne is composed of sands, silts, and clays. Silts and clays can contain carbonaceous material, as well as occasional lignite beds (Nelson, 1998). In ascending order, the Claiborne is separated into the Carrizo Sand, Cane River Formation, Sparta Sand, Cook Mountain Formation, and Cockfield Formation (the Carrizo and Sparta comprise the Memphis Sand in Tennessee), but thins northward in the Mississippi Embayment, where it is undifferentiated. In the CUSSO well, the base of the Claiborne is picked at the base of a dense or cemented sand at 268 m depth that also shows sharp changes in gamma-ray and resistivity logs (Fig. 3). This is similar to the base of the Claiborne picked in the nearby Florence No. 1 Smith well by Davis and others (1973).

Wilcox Formation (Upper Paleocene–Lower Eocene). The Wilcox Formation consists of sands, silts, clays, and gravels with some lignite at various locations. Sands are fine to very fine grained; clays are often sandy and silty with occasional carbonaceous inclusions. The top and bottom of the Wilcox Formation are regionally unconformable. In the CUSSO well, the top of the Wilcox Formation is picked beneath a thick sand with a cemented base at approximately 268 m. The base of the Wilcox is picked at the top of a hard, thick, black silty clay at 396 m, which also shows distinct changes in gamma-ray and resistivity responses (Fig. 3).

Porters Creek Clay (Early Paleocene). Below the Wilcox, the Midway Group consists of the Porters Creek Clay. The Porters Creek lies unconformably below the Wilcox Formation and is composed of a hard clay with glauconitic sands common in its upper and lower parts (Olive, 1980). In the CUSSO well, the top of the Porters Creek Clay is picked in the driller's log at the top of a hard black shale at approximately 396 m depth, which is a distinctive lithology for the unit. This contact exhibits sharp gamma-ray and resistivity responses in the wireline logs (Fig. 3). The base of the Porters Creek is picked on the geophysical logs at the base of a sequence of clay-dominant sediment, above a sandy clay at approximately 488 m depth (Fig. 3). This is similar to the top and base picked by Davis and others (1973) in the nearby Florence No. 1 Smith well, and for reasons of practicality, separates the thick clay interval from underlying mixed clays, silts, and sand. The underlying Clayton Formation contains clays, silts, and sands similar to those that can occur in the Porters Creek Formation, so the contact should be considered approximate. Palynological analysis would be needed to confirm the boundary.

Clayton-McNairy Formations (Late Cretaceous). The undifferentiated Clayton-McNairy Formation is a loose to friable micaceous sand with interbedded clays and silts. Sands in the Clayton and McNairy are lithologically indistinguishable so were commonly mapped together in the region (see, for example, Finch, 1971). At the CUSSO site, the undifferentiated Clayton-McNairy Formation extends from the unconformable top of hard sandy clay at approximately 488 m depth to the bedrock unconformity at 585 m, where resistivity increases sharply (Fig. 3). This is similar to the correlation of undifferentiated Clayton-McNairy Formation in the Florence No. 1 Smith well by Davis and others (1973).

Paleozoic Bedrock. Bedrock was reached at 585 m depth in the well. Fragments of rock noted at the basal unconformity likely represent weathered rubble. The borehole was advanced to 595 m in the underlying carbonates, but drilling fluid loss and rod drop likely associated with karst terminated the borehole. Top of Paleozoic bedrock at the CUSSO site is part of the Upper Ordovician Knox Supergroup, based on regional mapping (Potter and Pryor, 1961; Schwalb, 1969).

Site Geology

General. The lack of outcrop exposure in the Mississippi River Valley requires the subsurface geology to be determined using active or passive exploration geophysical techniques, as well as invasive drilling. The CUSSO site geology was determined using active high-resolution seismic-reflection (and -refraction) surface methods, as well as downhole geophysics and stratigraphic logs of the deep borehole. Seismic-reflection data were collected in east–west-oriented (lines UK-1, UK-1a, and UK-2) and north–south-oriented (UK-3) seismic-reflection profiles along rural roads within a 1-km radius

of the CUSSO site in order to define the geometric configuration for the major (i.e., high impedance) seismostratigraphic boundaries (Fig. 5). These 12-fold data were recorded with a 24-bit engineering seismograph using P-wave energy generated from a 4-kg hammer and 15 cm × 15 cm hardened aluminum plate. Five vertical hammer strikes were stacked at each shotpoint. In addition, two different receiver array geometries were used in order to optimally image both the relatively deep and shallow target stratigraphy. Specifically, a 10-m group/shot interval and 100-m near-offset source were used in lines UK-1, UK-2, and UK-3 to optimally image reflections from the tops of the deeper Cretaceous (K) and Paleozoic bedrock (Pz) stratigraphic horizons (Figs. 3–4); however, a reduced 2-m array interval and 50-m near-offset source were used for line UK-1a. The smaller array dimension for the latter profile produced better reflected images for the Tertiary and base of the Quaternary stratigraphic horizons. A conventional processing procedure was applied to all profiles, and included bandpass filters, gain correction, residual statics, coherent noise mutes, and iterative velocity analysis. Frequency-wavenumber filtering, adaptive subtraction, frequency-offset deconvolution, and post-stack Kirchhoff depth migration were also applied. The overall signal from the data set exhibited an average dominant frequency of 50 Hz and average velocity of 1,900 m/s. This yielded vertical and detectable resolutions of approximately 9.5 and 4.5 m, respectively.

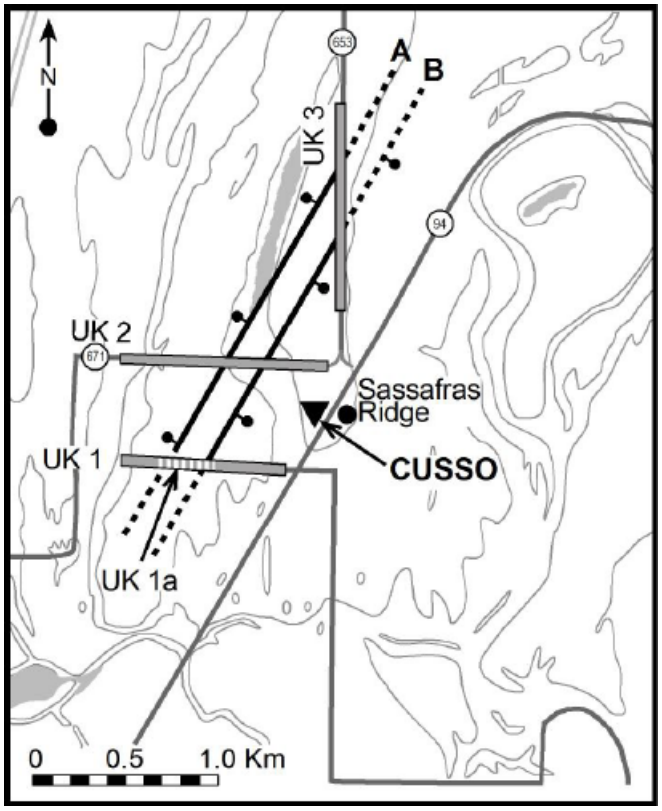

Figure 5. The seismic-reflection profiles are located in a small rural community, called Sassafras Ridge (black-filled circle), which sits atop a subtle topographic rise within the Mississippi River floodplain. The seismic lines were collected in a 1-km radius of the CUSSO borehole (black-filled triangle) that penetrated 585 m of Quaternary (Q), Tertiary (T), and Late Cretaceous (K) sediments and terminated in the underlying Paleozoic (Pz) bedrock. Lines UK-1, UK-2, and UK-3 (heavy gray lines) imaged the deeper K and Pz horizons. Line UK-1a (white dashed line) was collected coincident with part of line UK-1, but was designed to image the shallower Tertiary and basal Quaternary sediments. The heavy black lines labeled A and B approximate the boundaries of an imaged pop-up horst feature that was correlated between the seismic lines. The labels are indexed to the fault interpretations on lines UK-1, UK-2, and UK-3. Highways are dark gray lines (identifying numbers in circles). Topographic contours are shown in light gray.

Lines UK-1 and UK-1a. Line UK-1 is a 650-m east–west-oriented profile collected along a level road 0.25 km south of CUSSO (Figs. 5–6). The two most prominent reflections are from the tops of the K and Pz stratigraphic horizons; their seismic migration depths agree with borehole data. Figure 6 shows the uninterpreted and interpreted seismic-reflection profiles. Although the reflections above the K horizon have weaker and more discontinuous characteristics, the Porters Creek and Wilcox formations are relatively coherent across the profile. These stratigraphic interpretations also correlate with information from the adjacent borehole. A near-vertical fault was interpreted crossing the monoclinal flexure of the K and Pz reflectors near UK-1's trace number 80—labeled "A" in the lower part of Figure 6c. The fault affects the overlying horizons, including the Wilcox and younger strata. Vertical relief across this structure is approximately 50 and 75 m on the K and Pz horizons, respectively. A smaller fault is interpreted near trace 55—labeled "B" in the lower part of Figure 6c. This feature has an estimated eastern downthrow of approximately 30 m for both the K and Pz horizons. As a composite, the shallower uplifted reflectors between faults A and B are arched and define a narrow, upward-

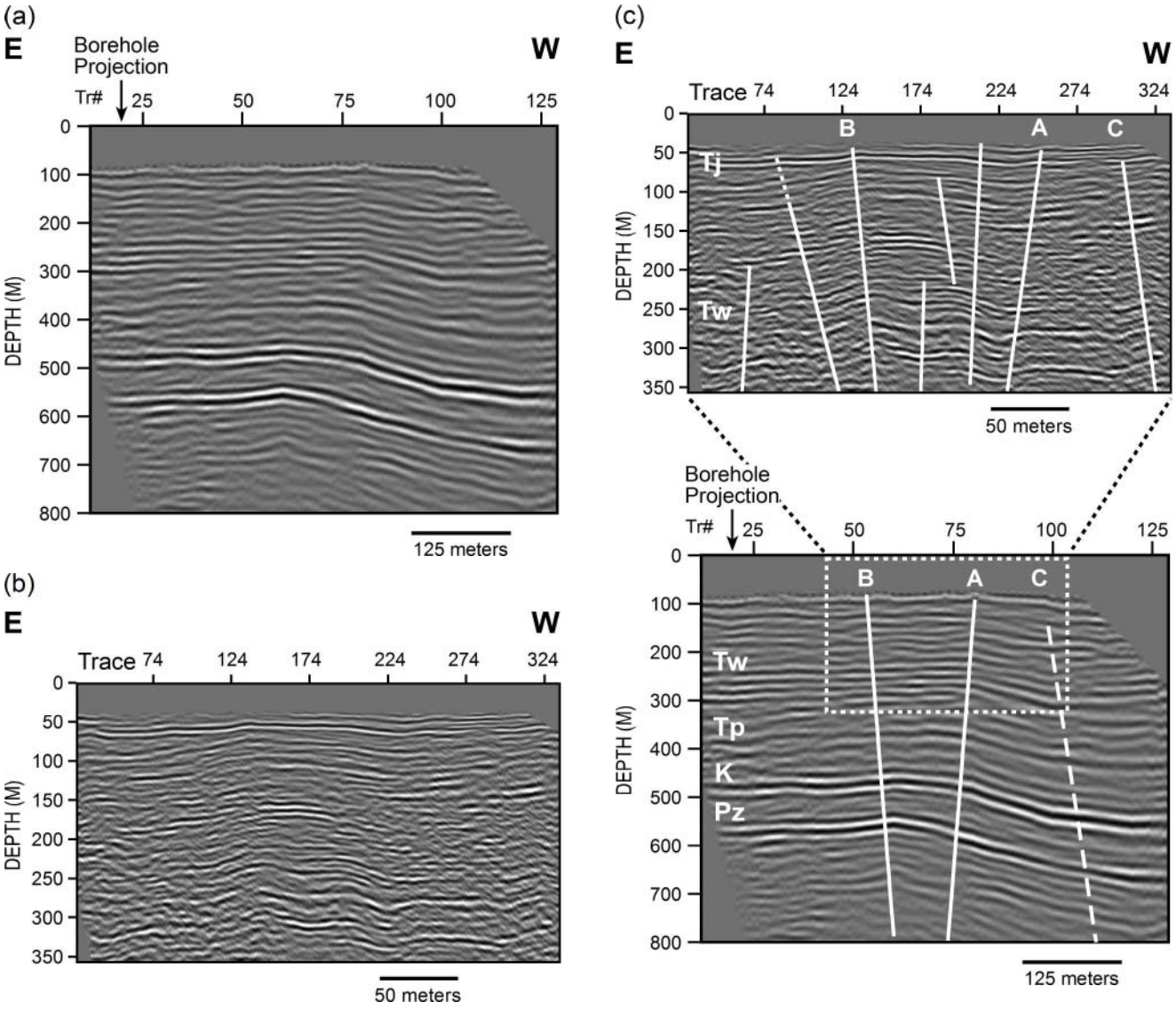

Figure 6. Uninterpreted stacked profiles of the east–west-oriented lines (a) UK-1 and (b) UK-1a. The profile locations are shown in Figure 5. (c) The spatial relationship between the interpreted UK-1 and UK-1a lines. Line UK-1 was arrayed to target the deeper K and Pz stratigraphic horizons. Line UK-1a was collected coincident with part of line UK-1 using a shorter array spacing in order to better image the shallow stratigraphy and structure within the zone defined by the white dashed rectangle. The pop-up structure, bounded by high-angle faults A and B, offsets the Jackson Formation (Tj) and deforms the base of the Quaternary sediment. Another fault, C, has a more pronounced expression in line UK-1a than in line UK-1.

splaying, asymmetric pop-up or horst structure. A fault is also interpreted at trace 100—shown as a dashed line and labeled "C" in the lower part of Figure 6c—based on the abrupt change in the dip of the reflections, as well as a small reversed displacement. The fault C deformation in this profile is very subtle across the K and Pz horizons. The fault would not be interpreted if not for the dip changes in the shallower reflections and the projection of a fault to this approximate station in the more definitive structural observations made in the other profiles. It is also possible that the primary deformation associated with the deeper part of fault C is located off the western end of line UK-1. Without additional data acquisition, the reliability of the fault C interpretation is unknown.

Line UK-1a was acquired coincident with a part of line UK-1 and across its interpreted structure (Fig. 5). The 330-m-long survey, shown in Figure 6b and the upper part of Figure 6c, was arrayed

to better image the Tertiary and basal Quaternary horizons. The stacked data set is rich in reflected signals; however, the two most prominent and continuous reflections are from the Wilcox and Jackson Formations. The primary faults, A and B, imaged in line UK-1 are also exhibited at the coincident line UK-1a stations. The imaged faults appear to cross the Jackson Formation, displacing the base of the Quaternary. The tops of the Wilcox and Jackson horizons have as much as 25 and 15 m of vertical relief, respectively. The near-surface structural characteristics also show arched reflectors bounded by two primary near-vertical faults, A and B, that diverge upward, similar to that imaged in line UK-1. The structure exhibited in the more detailed UK-1a image has characteristics consistent with a strike-slip-induced pop-up or flower structure. Line UK-1a also shows the extension of fault C into the near-surface sediment. The abrupt change in dip and reversed displacement is more clearly resolved in this image than in line UK-1.

Line UK-2. Line UK-2 is an 800-m-long, east–west-oriented profile (Fig. 7) collected 0.20 km north of CUSSO (Fig. 5). This profile was arrayed to image the deeper K and Pz target horizons. The reflections above the K horizon are more discontinuous than the K or Pz horizons; however, the reflections from the tops of the Porters Creek and Wilcox formations appear relatively coherent across the profile and correlate with the interpreted borehole stratigraphy. Two near-vertical faults are interpreted near trace numbers 90 and 45, based on the antiformal warping of the K and Pz horizons, as well as vertical elevation differences and abrupt dip changes on either side of fault traces. These faults are labeled A and B, respectively. The composite structure is interpreted as the same pop-up feature imaged along lines UK-1 and UK-1a. The K and Pz horizons appear to have nearly 45 and 70 m of offset, respectively, somewhat less than that estimated on line UK-1; however, as in line UK-1, the largest vertical relief appears on the western side of the structure (i.e., fault A). A third near-vertical fault, labeled C, is interpreted at trace 125, but it has less offset than (approximately 30 m) and an opposite throw (west side up) as fault A. Nonetheless, the measured fault C vertical offset in this line is more than that observed in line UK-1. All faults appear to deform the Tertiary horizons.

Line UK-3. Line UK-3, a 900-m-long, north–south-oriented profile (Fig. 8), was collected 0.30 km northeast of CUSSO (Fig. 5). This survey targeted the deeper horizons; however, unlike on lines UK-1 and UK-2, the top of the Porters Creek is the most prominent reflection observed on the UK-3 profile. Although visible, the typically strong K and Pz reflections are relatively weak and less coherent in line UK-3 than in lines UK-1 and UK-2. Near-

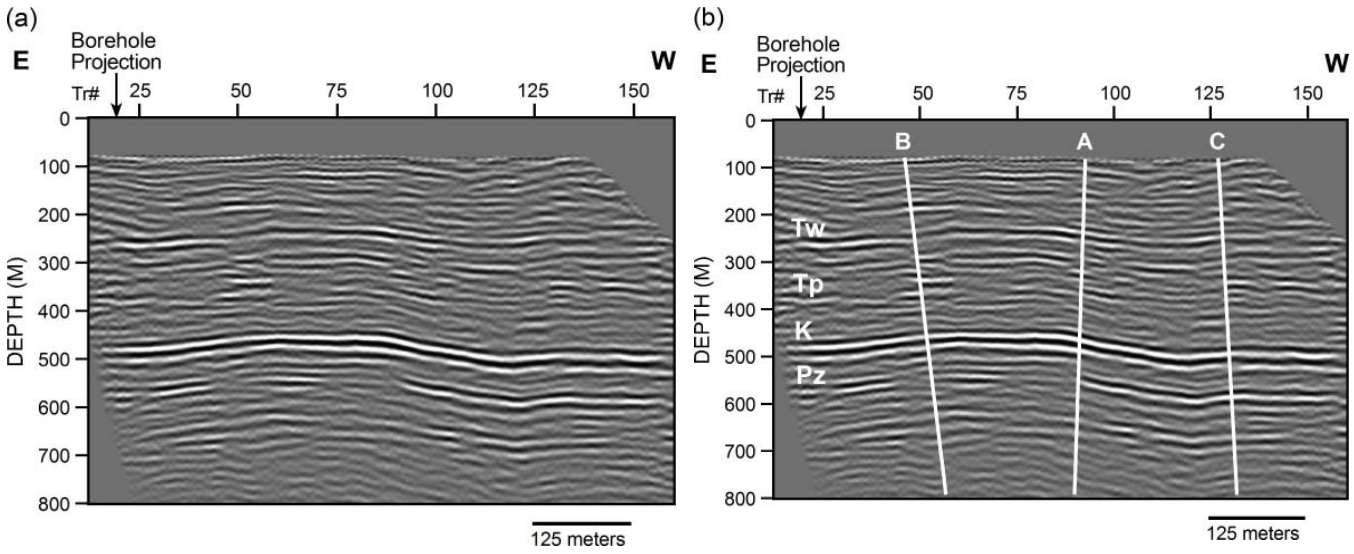

Figure 7. (a) Uninterpreted and (b) interpreted stacked profile of the east–west-oriented line UK-2. The line's location is shown in Figure 5. The pop-up structure, bounded by high-angle faults A and B, displaces the Pz and K reflectors, and deforms the resolved Tertiary sediments. Fault C, near the end of the profile, also disturbs Tertiary sediments.

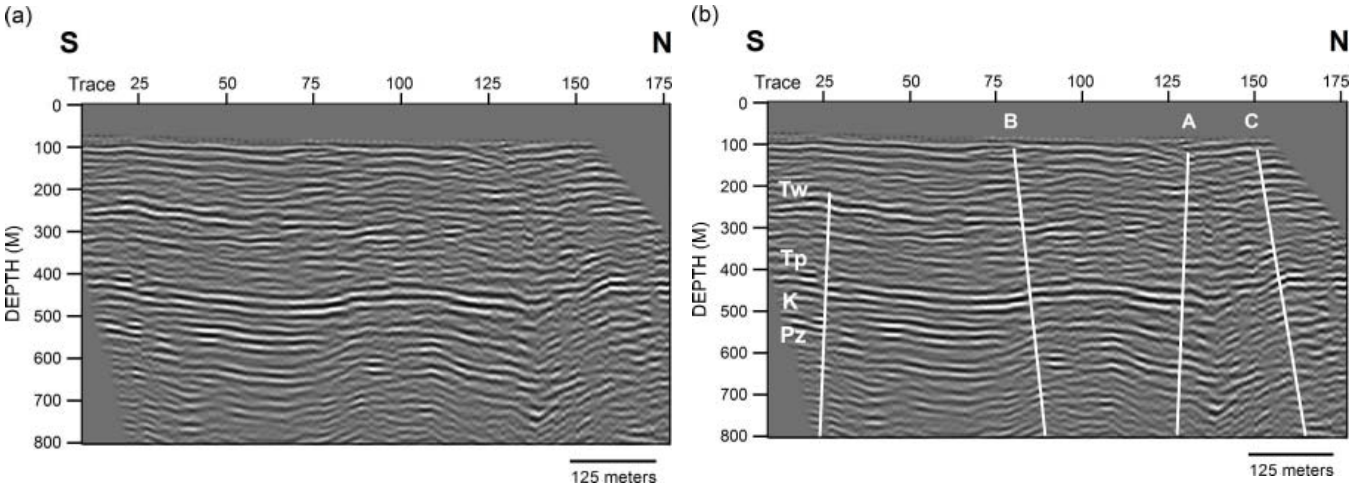

Figure 8. (a) Uninterpreted and (b) interpreted stacked profiles of the north–south-oriented line UK-3. The line's location is shown in Figure 5. The prominent pop-up structure is located between traces 80 and 130 (labeled B and A, respectively), and extends above the Pz, affecting all resolvable stratigraphic horizons. Fault C, located at trace 150, exhibits more deformation here than in lines UK-1 and UK-2.

vertical faults are interpreted at traces 130 and 80, bounding a region of uplifted strata that exhibits antiformal folding. These faults are labeled A and B, respectively. Both faults A and B cross the reflected tops of the Pz, K, and Porters Creek, as well as affect the overlying horizons, including the Wilcox and younger strata. The largest amount of vertical relief occurs across fault A, on which there are 50 and 75 m of displacement on the K and Pz horizons, respectively. The Porters Creek also exhibits nearly 50 m of structural relief. The reflectors in the area bounded by faults A and B are uplifted and antiformally warped, comparable to and interpreted to be the northeast continuation of the flower structure imaged on lines UK-1 and UK-2. Another evident and significant deformation consisting of two faults, labeled C, is at trace 150, near the northern end of the line (Fig. 8). Fault C displacement has a pronounced apparent southern downthrow of approximately 50 m on the Tp horizon; however, weakened signal deeper in the record precludes a definitive estimate of offset along the K and Pz horizons. This is the largest observed vertical offset for fault C at the site. We also interpreted a fault at trace 30 near the southern end of the profile. It is near vertical with approximately 20 m of displacement and projects just off the eastern ends of lines UK-1 and UK-2 using a strike equivalent to that defined by faults A and B.

Geologic Site Interpretation and Broader Context. These seismic-reflection images exhibit a set of steeply dipping faults that have uplifted and arched post-Paleozoic sediments in a manner consistent with positive flower structures found in dextral strike-slip displacement, and similar to transpression features interpreted in other regional seismic profiles (see, for example, Van Arsdale and others, 1995; Odum and others, 1998). This local fault zone strikes approximately N30°E and was correlated 1.4 km between the reflection surveys; however, these data are too closely spaced for a meaningful regional scaled inference. Nevertheless, Woolery and Almayahi (2014) projected the structure northeast along strike approximately 22 km to its intersection with a lower-resolution reflection profile (M-21) in an initial evaluation of the areal extent (Fig. 9). The reflection image at the site of the intersection revealed a discrete set of upward-splaying, high-angle faults that bounded a subsurface area with an uplifted and arched K reflection (Fig. 10). This approximately 750-m-wide zone has a comparable style to the approximately 200-m-wide structural feature imaged on the high-resolution seismic-reflection profiles acquired at the CUSSO site. The increase in structural width is perhaps by geomechanical interaction or diffusion with the larger, broader structure immediately north in the profile; however, it may be an artifact of the

horizontal resolution, a changing strike, or an incomplete imaging of a broader structure at the CUSSO site. Woolery and Almayahi (2014) recognized that lines UK 1 through UK-3 were too closely grouped for them to make an indisputable regional structural interpretation, but they also recognized that their significant separation from the industry data also make a correlative interpretation equivocal. The current data set is kinematically indicative of a significant regional transpression structure. The high-resolution data also show that structural relief extends above Pz bedrock, crossing the K and T horizons and base of the Quaternary sediments. Woolery and Almayahi (2014) also noted that the site's aforementioned subtle topographic high (approximately 3 m) may be a result of structural influence; however, this relationship is speculative and requires further higher-resolution study (i.e., ground-penetrating-radar, shallow drilling, trenching, etc.). The Pz and K horizons, however, show as much as 75 and 50 m of structural relief, respectively, with the middle Eocene and basal Quaternary displaced 25 and 15 m, respectively. The interpreted fault orientation and deformation style at the CUSSO site and the positive regional correlation with the industry data suggest a northeast-oriented transpression structure orthogonal to the Reelfoot stepover and along the central embayment axis. Woolery and Almayahi (2014) stated that the structure is too far inboard to have an association with northeast-oriented Reelfoot Rift margins, but is coincident with the projection of the northeast-oriented Axial Fault, the structure responsible for the dense, narrow band of seismicity extending between northeastern Arkansas and southwesternmost Kentucky. Consequently, they interpreted these newly discovered faults to be part of a hypothesized northeast-oriented shear zone extension that crosses the New Madrid left-stepover thrust (Pratt and others, 2012). If Pratt and others (2012) are correct, their interpretation extends the shear zone a minimum of 34 km. The interpretation by Woolery and Almayahi (2014) would also provide for the continuation of the northeast-oriented, partitioning strike-slip faults in the hanging wall of the central stepover Reelfoot thrust into the footwall interpreted by Odum and others (1998). Modeling and analog comparisons for the New Madrid stepover structure by Pratt (2012) also resulted in a kinematic framework that included a major northeast-oriented shear zone, although it was located in Missouri, northwest of our site. Consequently, the geologic structure at CUSSO potentially reveals the first physical evidence consistent with recent model- and observation-based hypotheses regarding strain accommodation. In addition, it provides well-constrained location and geometry for faults

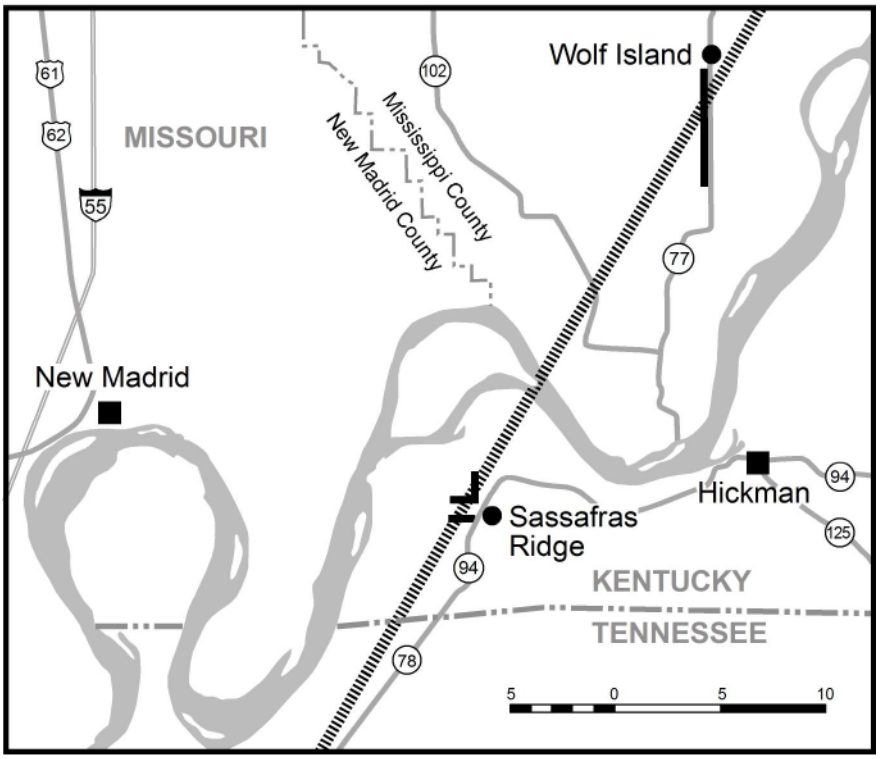

Figure 9. Relationship of the transpressional feature (short-dashed line) interpreted between the high-resolution lines UK-1, UK-2, and UK-3 (black lines at Sassafras Ridge) and the lower-resolution line M-21 (black line at Wolf Island). Although additional data are required to better validate the spatial and temporal relationships, the shear zone hypothesized by Pratt and others (2012) has been extrapolated here to pass beneath CUSSO. The northeast-oriented transpressional structure interpreted at CUSSO is potentially the first corroborative physical evidence for this hypothesized shear zone crossing the New Madrid Seismic Zone's left-stepover arm, and accommodating the unbalanced strain between the Reelfoot Fault and scarp.

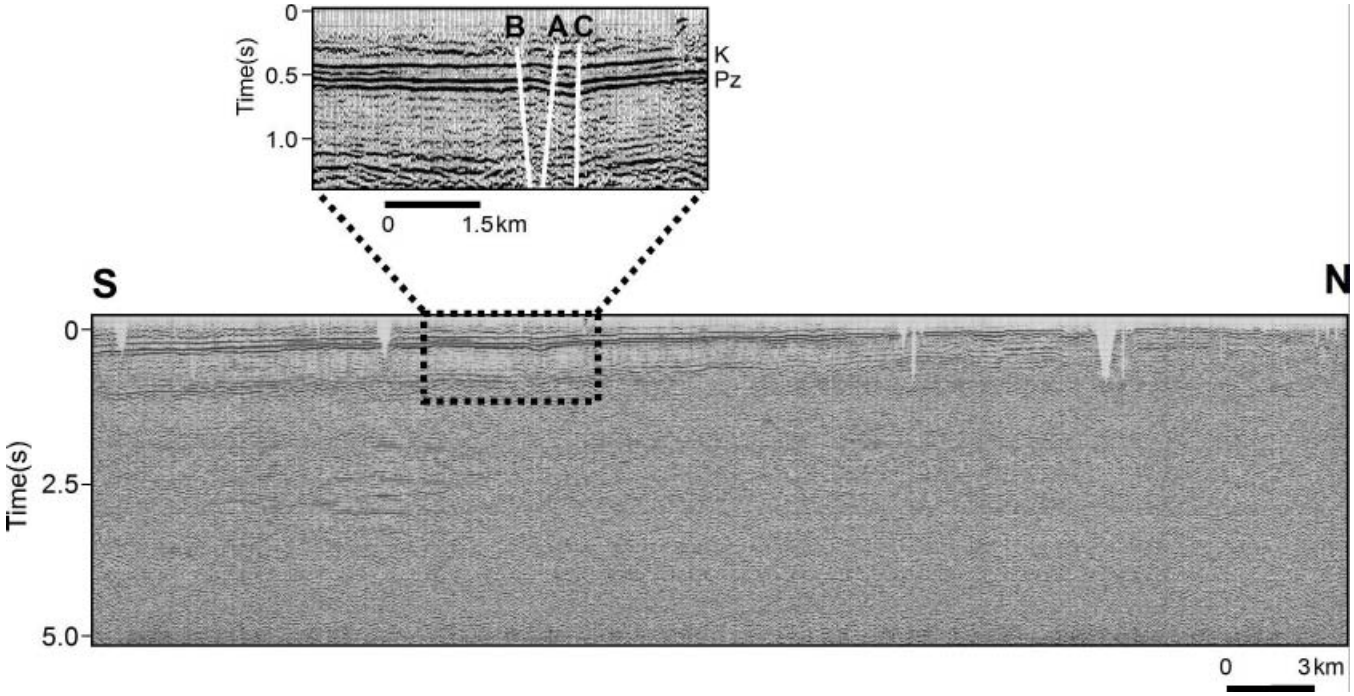

Figure 10. Dow Chemical's Vibroseis line M-21, oriented north-south along the Mississippi River floodplain in southeastern Missouri. The 6-km area surrounds the point of structural intersection with the projected N30°E strike defined by the high-resolution seismic-reflection profiles of this study. High-angle, upward-splaying transpression faults similar to those identified in lines UK-1, UK-2, and UK-3 are at the projected structural intersection. The Dow data are much lower resolution, but reveal uplifted and antiformally warped Pz and K reflections similar to those imaged in the higher-resolution data. The Dow line is displayed in two-way travel time (i.e., not depth converted). Used with permission of the Apache Corp.

active in the Quaternary, thus providing more definitive spatial and eventual temporal parameters that can improve intraplate tectonic and seismic-hazard models for the central United States. More comprehensive geophysical and geologic study will be required to evaluate the spatial and temporal limits of these structures, as well as the range of their implications.

P- and S-Wave Velocity Models

The seismic velocity model at the site, shown in Figure 4, is composed of seven layers over a bedrock half-space (Brengman, 2014). The model was constructed from three primary sources: (1) surface seismic-reflection and -refraction surveys, (2) P- and S-wave suspension-velocity logs by Geovision Inc. of the total 595-m borehole depth, and (3) phase arrival times measured across the instrumented array. Woolery and Wang (2010) reported P- and S-wave velocity measurements from downhole velocity-suspension logs and surface seismic walkaway soundings. In addition, earthquake phase arrival observations between the surface and bedrock instruments provided bulk average S- and P-wave velocity measurements of 610 and 1,836 m/s, respectively, for the sediment column. Woolery and Wang (2010) also noted low-velocity inconsistencies between results of the suspension logs and the seismic walkaway soundings. Two zones of anomalously low velocity are exhibited from 50 to 130 m and 180 to 265 m below ground surface. These low-velocity zones are exhibited in both the P- and S-wave suspension logs, but more pronounced in the S-wave log. Although the suspension logs are not susceptible to blind zones and provide higher-resolution velocity measurements relative to the surface soundings, the two low-velocity zones indicated on the suspension logs are interpreted to be artifacts of the drilling process in the immediate vicinity of the borehole. Specifically, considerable instability and collapse of the borehole walls were noted during drilling; consequently, we speculate that the substantial sediment disturbance in the borehole annulus and immediate vicinity altered the velocity-suspension log measurements and produced results not in-

dicative of the true conditions. The average P- and S-wave velocity values measured from the phase observations are also similar to the average velocities found from the refraction and reflection walkaway sounding measurements (Woolery and Wang, 2010). We interpreted the average S-wave velocity to be approximately 300 m/s higher than the weighted average predicted by the suspension-log measurements. This also suggests that the suspension-velocity measurements are anomalous, and perhaps caused by sediment being disturbed around the borehole. The seven layers that make up the velocity profile correlate well with observed stratigraphic horizons: the lower boundary of layer 1 correlates with the top of the basal Quaternary gravel, and the lower boundaries of layers 2, 4, 5, 6, and 7 are at the interpreted basal boundaries for the Jackson, Claiborne, Wilcox, Porters Creek, and Clayton-McNairy formations, respectively.

Instrumentation and Operation

Configuration

CUSSO is a 21-component vertical seismic array with sensors deployed at various elevations between the surface and bedrock (Fig. 2). The subsurface instruments reside in three adjacent boreholes drilled to depths of 30, 259, and 595 m. These vertical arrays were constructed and instrumented in two phases: During the first phase in fall 2006, the 30- and 259-m-deep wells were drilled and instruments were installed, and during the second phase in fall 2009, the 595-m-deep well was drilled and instruments installed. The 259- and 595-m vertical arrays hold accelerometers and a seismometer at major impedance boundaries identified in the site characterization surveys, and the 30-m borehole houses an accelerometer that was specifically placed to correspond with the empirically defined dynamic site-coefficient boundary as defined by the Building Seismic Safety Council (2009). Consequently, the 30-m borehole was configured to evaluate the applicability of the current NEHRP ground-motion scaling factors derived from the time-averaged shear-wave velocity of the uppermost 30 m of strata. This shallow borehole was auger drilled and completed with 102-mm-diameter, schedule-40 PVC casing and an exterior tremie cement–bentonite backfill.

The 259-m intermediate arm of the array was instrumented with an accelerometer. This elevation was selected based on a strong impedance boundary identified in seismic-reflection walkaway soundings and common-midpoint profiles (Woolery and Wang, 2010, 2012; Woolery and Almayahi, 2014). Stratigraphically, this correlates with the base of the Memphis Sand, a lower unit of the Claiborne Group (Fig. 3). The borehole was drilled using a mud-rotary method and completed with 102-mm steel casing and an exterior tremie cement–bentonite backfill.

The deep borehole was advanced using a telescoped mud-rotary operation. An initial 38-cm-diameter borehole was drilled and cased to a depth of 46 m below the surface in order to stabilize the loose alluvium. The second part of drilling advanced a 25-cm-diameter boring through the remaining sediment. The total sediment thickness at the site was 585 m, and the borehole was terminated at a final depth of 595 m (approximately 10 m into rock). The drilling encountered considerable sidewall instability throughout the top 260 m, likely altering conditions in the neighborhood of the borehole annulus and affecting suspension-velocity measurements (see **Instrumentation and Metadata,** below). An accelerometer and seismometer were installed 2 m below the sediment-bedrock interface (i.e., at 587 m). An additional accelerometer was placed in the deep borehole at a depth of 526 m, immediately below the major velocity boundary that defines the top of the Clayton-McNairy Formations (Figs. 3–4).

Instrumentation and Metadata

The seismometer and accelerometer placement, in descending elevation, is (1) a medium-period seismometer and strong-motion accelerometer at the surface, (2) a strong-motion accelerometer at 30 m, (3) a strong-motion accelerometer at 259 m, (4) a strong-motion accelerometer at 526 m, and (5) a medium-period seismometer and strong-motion accelerometer within the bedrock at 587 m. The medium-period seismometers have flat responses to ground velocity between 0.067 and 50 Hz. Some of the strong-motion accelerometers have full-scale acceleration thresholds between 0.25 and 1.0 g, and the others have a full-scale acceleration threshold of 2.0 g. All have nominal corner frequencies of 50 Hz, except one has a nominal corner frequen-

cy of 200 Hz. The 21 components are recorded by a data logger. The system consists of 32 channels configured with unity gain and variable full-scale input voltages, 24-bit data, and an anti-aliasing filter. The anti-aliasing filter is a double-precision, finite-impulse, response acausal filter, which attenuates the output by more than 140 dB at the Nyquist frequency.

Installing the borehole sensors in multiple cycles was a problem, because these sensors lack internal compasses; thus, the orientations of their horizontal components were unknown, and likely differed for each reinstallation. During the period of peak earthquake activity (December 20, 2010–April 27, 2011), however, all borehole-sensor orientations were estimated by cross-correlating long-period waveforms (i.e., periods greater than 4 s, which are not significantly modified as they ascend the sediment column) from teleseismic earthquakes recorded by the borehole sensors' transverse components, with the east component recording at the surface (Brengman, 2014).

The metadata, including instrument responses, for the CUSSO array was assembled in dataless SEED format, incorporating vendor-supplied sensor calibrations (Brengman, 2014). The accuracy of the instrument responses was verified by comparing long-period observations from CUSSO with recordings from nearby calibrated stations (Fig. 11a), and then comparing CUSSO recordings of long-period phases at each component (Fig. 11b). Long-period waveforms (periods greater than 4 s) recorded in the vicinity of CUSSO underwent limited to no amplification from resonance and decreasing velocity up the sediment column. Also, the effect of the free-surface was uniform at longer periods (wavelengths greater than four times the sediment thickness) at all depths (Shearer and Orcutt, 1987).

Operational History

Operation of the full CUSSO array has been interrupted multiple times since its installation by either failure of a deep-hole sensor or a connector (526-m and 587-m sensors) or by sheared cable from high hydrostatic pressures (approximately 850 psi at 587 m). The sensors at the surface, 30 m, and 259 m also had occasional problems related to damage from lightning strikes and various mechanical issues. Figure 12 summarizes CUSSO's operational history, focusing on the period from the installation of the deep-hole sensors through the most recent reinstallation attempt, and the earthquakes it recorded while the deep-hole sensors were installed. The most recent attempt to reinstall the bedrock sensors was in June 2013; however, within a few hours of the installation, the signal was interrupted because of a pressure-induced cable failure.

Originally, the data logger at CUSSO was configured to operate in trigger mode only, recording all channels at 200 samples per second. Event triggering continues, but in October 2012, the University of Kentucky also began acquiring data from CUSSO in real time; in June 2013, the sample rate was reduced to 100 samples per second.

Recordings

Despite the instrumentation problems, the array has recorded 95 earthquakes at local (24 earthquakes; offsets less than 130 km; magnitudes from 1.3 to 3.1), regional (37 earthquakes; offsets from 300 to 1,550 km; magnitudes from 2.4 to 5.2), and teleseismic (34 earthquakes; offsets greater than approximately 20°; magnitudes from 5.0 to 9.0) distances (Fig. 13). We analyzed earthquake recordings acquired from November 2009 through April 2011, when for all but approximately 3½ months, at least one of the bedrock sensors was operational (Fig. 12). Notably, the array recorded 33 earthquakes in the 2010-11 Guy-Greenbrier earthquake swarm (Arkansas). We examined waveforms, amplitude spectra, and spectral ratios within the frequency band of engineering interest (0.1 to 20 Hz), which coincides with the frequency band of consistently useful data (i.e., instrument noise commonly dominates CUSSO's weak-motion accelerometer recordings for frequencies outside this band). However, no CUSSO records contain strong ground motions; very few recorded amplitudes exceed 1 cm/s^2. The peak acceleration recorded to date is 1.8 cm/s^2 from an M 3.1 earthquake 22 km away. The numerous weak-motion recordings yielded high-quality observations, however.

Waveforms from the largest event in the Guy-Greenbrier earthquake sequence, an M 4.7 earthquake on November 28, 2011, are shown in Figure 14 as an example of earthquake waveforms recorded by the full array. Although CUSSO was

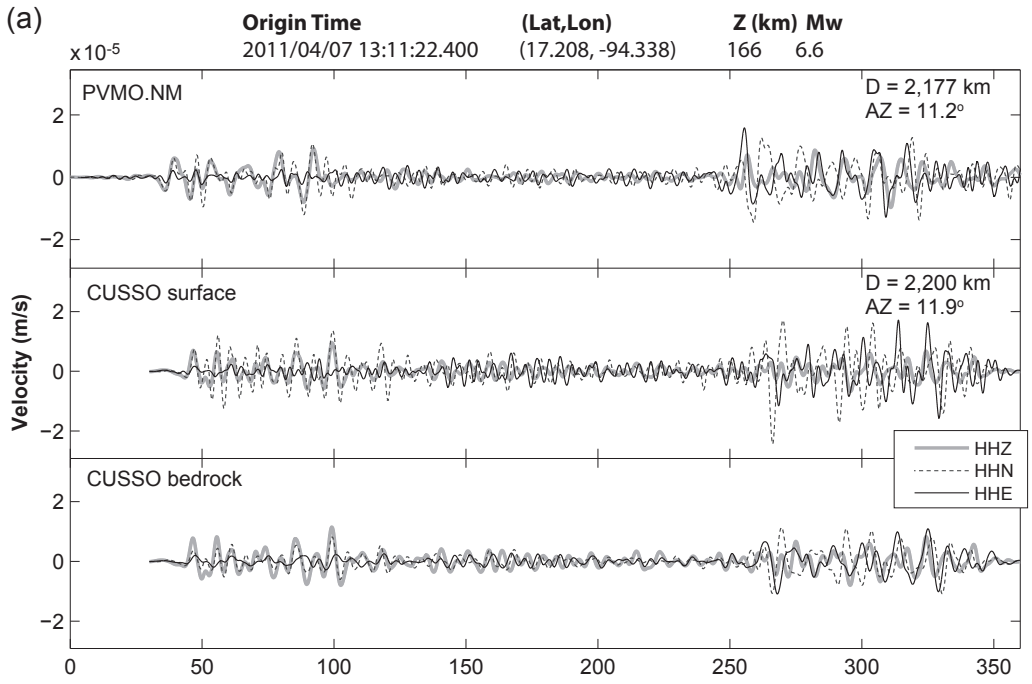

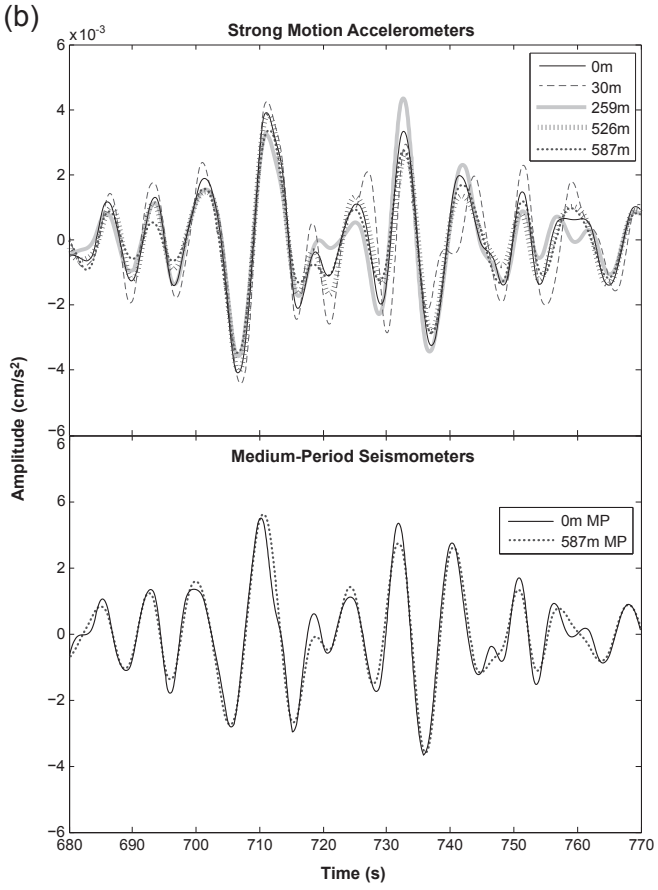

Figure 11. (a) Vertical, north, and east seismograms from an M_w 6.6 teleseismic earthquake recorded by the calibrated station PVMO (New Madrid network, operated by the Center for Earthquake Research and Information at the University of Memphis; top) and CUSSO's surface (middle) and bedrock (bottom) seismometers. Data are bandpass-filtered to within the passband of all sensors, which equalizes amplification from the vertically ascending waves at CUSSO (0.07 and 0.2 Hz), and are corrected for the effects of the instruments. The similarity in the amplitudes and waveforms, also observed at other nearby CERI stations, indicates that CUSSO's instrument responses are correct. (b) S-wave arrivals from the M_w 9.0 Tōhoku earthquake (March 9, 2011) recorded on the (rotated) transverse components of CUSSO accelerometers (top) and seismometers (bottom), filtered from 0.07 to 0.2 Hz, with the effects of the instruments removed. The similarity in these waveforms recorded by the various instruments supports the accuracy of the instrument responses and the calculated sensor orientations.

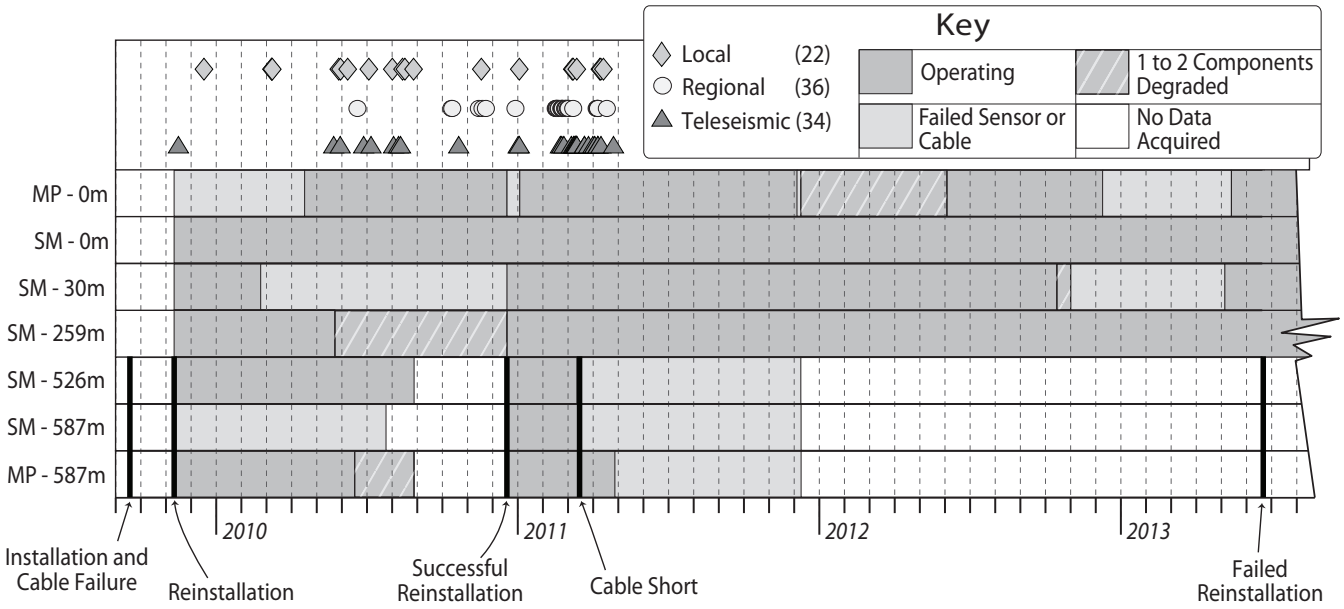

Figure 12. Summary of CUSSO's history, focusing on when the deepest borehole sensors recorded earthquakes, including recorded earthquakes (top) and the operational status of each sensor during this time (lower grid). MP = medium-period seismometer; SM = strong-motion accelerometer. Events of significance in CUSSO's deep borehole are indicated with a heavy, black line and labeled. The time span also includes the most recent attempt at reinstallation in June 2013. The array status following the 2013 failed reinstallation continues through the present, as shown.

too far from this earthquake (308 km) to record strong ground motion, the signal quality is good and exceeded the noise across our frequency band of interest (Fig. 15). Figure 16 shows vertical-component waveforms of P- and S-phase arrivals from the bedrock to the surface from an M 2.3 earthquake 22 km west of CUSSO. Multiple P-wave and sP (S-to-P converted phases at the sediment-bedrock interface) reflections—upgoing and downgoing—are apparent in the waveforms.

Spectral ratios from the CUSSO recordings provide additional insight into seismic-wave propagation and modification through the sediment overburden. Figure 17 plots ratios of S-wave amplitude spectra (HH) between each adjacent instrumented interval for three of the best-recorded (i.e., clearest signal) earthquakes, including the two with the largest ground motions, to estimate four transfer functions in the instrumented intervals between the bedrock and ground surface. The earthquakes, ranging in magnitude between 2.7 and 4.7, occurred at back azimuths between 240 and 360°, and at distances between 22 and 308 km. Horizontal-component amplitude spectra are calculated from the square root of the sum of the squares of the orthogonal horizontal components, and the ratios are smoothed with a running average using a 0.5-Hz Hanning window. The transfer functions generally are consistent between the events. Beginning with the deepest interval (Clayton-McNairy Formations), there is a small amplification factor of approximately 1.5 between the bedrock and 526 m. The second interval, between 526 and 259 m, is primarily composed of the Porters Creek Clay and Wilcox Formation. The amplitude response for this section is markedly frequency-dependent; specifically, below approximately 2 Hz there is an average amplification factor of approximately 2, but amplification decreases above 2 Hz, and amplitudes are attenuated for frequencies above 7 Hz. The third interval, between 259 and 30 m, is primarily composed of the Claiborne Group and Jackson Formation. Similarly to the previous interval, amplitudes for these sediments are also amplified by a factor of approximately 2; however, two spectral peaks emerge at 1.1 and 3.2 Hz, suggesting resonance is established within the Claiborne-Jackson. The near-surface interval, between 30 m and ground surface, is of late Quaternary age. Frequencies are largely unamplified, or even attenuated, below 1 Hz; however, for frequencies above 1 Hz, a distinct frequency-dependent amplification occurs, as

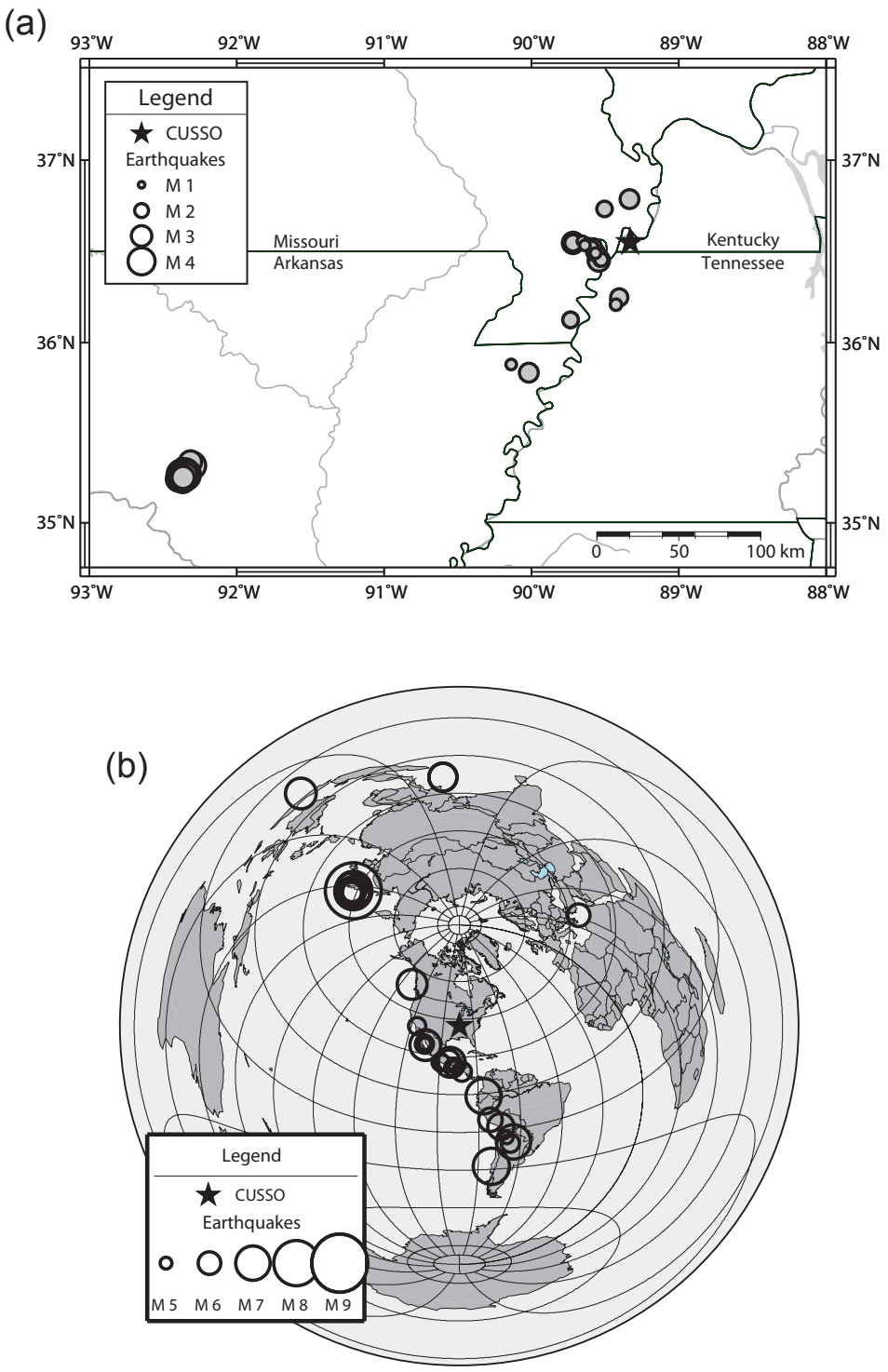

Figure 13. (a) Local and regional and (b) teleseismic earthquake locations recorded from CUSSO's original installation through the April 2011 failure of sensors in the deep hole (526 m and 587 m).

indicated by three dominant spectral peaks at 2, 5.5, and 11 Hz. In addition, there is a general increase in response at frequencies above approximately 5 Hz. The frequencies for the first two spectral peaks are consistent with the fundamental (1.8 Hz) and first-harmonic (5.4 Hz) frequencies estimated from the average shear-wave velocity between the ground surface and 30 m (Fig. 4). The interval shown in Figure 17 also illustrates the potential for noise to adversely affect a spectral-ratio calculation. For example, the signal-to-noise ratio in these recordings is approximately 1 for the 30-m and 259-m accelerometers across all frequencies; consequently, the increased low-frequency noise at 30 m relative to the surface results in an artificially low HH (i.e., noise suppression) for the M 2.7 event at frequencies below 10 Hz.

We also determined horizontal-to-vertical spectral ratios (HV) of the S-wave window for the same three earthquake surface recordings used in the HH calculations (Fig. 18). A comparison of HH and HV indicates distinct low-frequency spectral peaks at approximately 0.3 and 0.8 Hz. These peaks occur in each event, with minor spectral shifts. The most notable shift in HV response occurs for the M 4.7 event, which is lower than for other events; however, this lower peak more closely correlates to the theoretical fundamental frequency for the entire sediment column, including observed HH results.

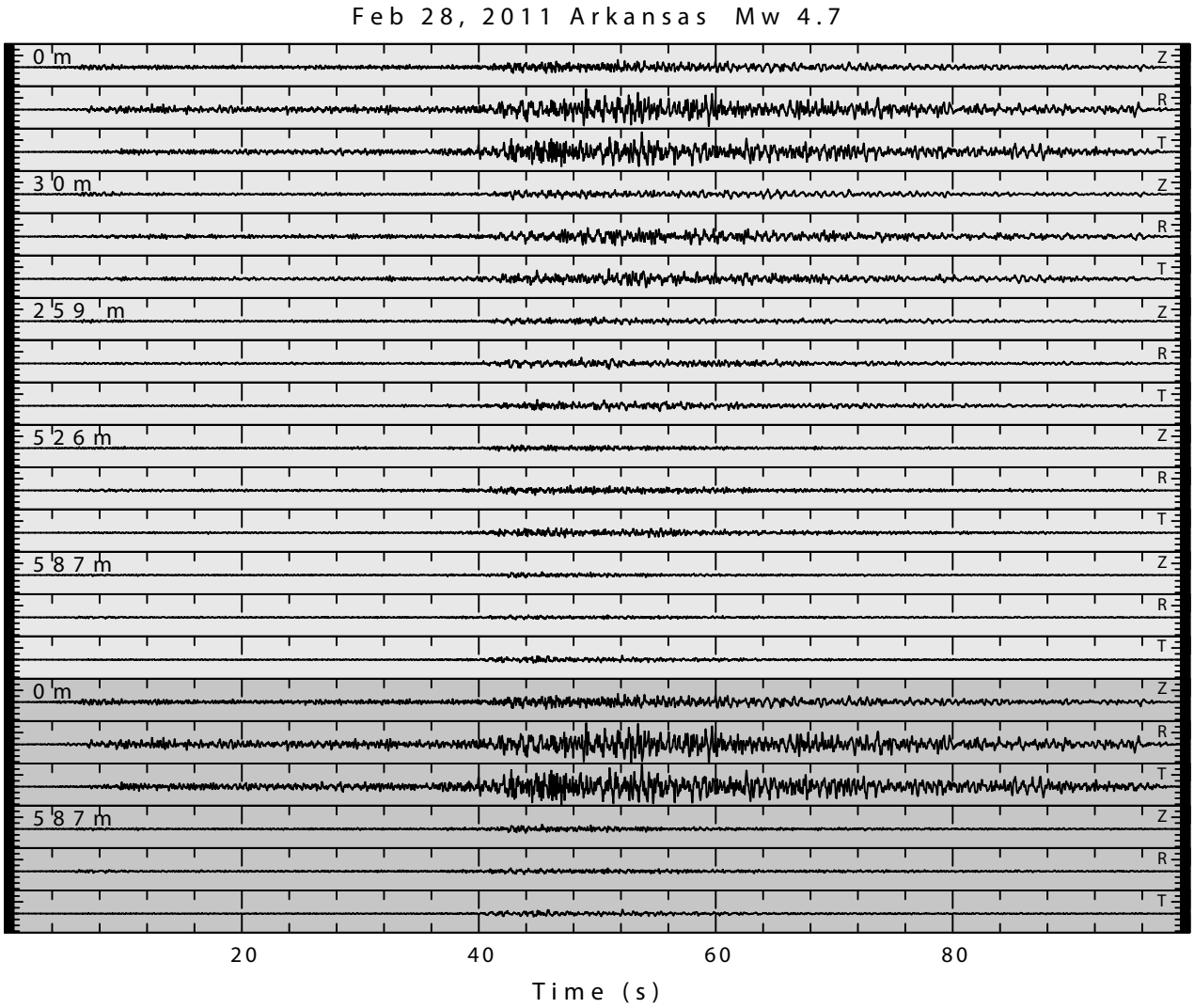

Figure 14. Waveforms recorded on the full CUSSO array from the M4.7 Arkansas earthquake of Feb. 28, 2011, 308 km to the west-southwest. Traces are instrument-corrected, the horizontal components rotated to radial and transverse orientations, and the data bandpass filtered from 0.5 to 12 Hz. All traces are scaled to the maximum amplitude of approximately 0.8 cm/s^2. Strong-motion accelerometer recordings have a light background, and seismometer recordings have a darker background.

However, the frequencies at which all these peaks occur are generally consistent with the fundamental frequency (0.26 Hz) and first harmonic frequency (0.78 Hz) estimated for the total overburden. We also found that the average spectral ratios (i.e., amplification) are only consistent within a narrow band between 0.3 and 1.1 Hz; at lower frequencies (i.e., less than 0.3 Hz), HV is consistently more amplified than HH is, whereas at higher frequencies (i.e., greater than 1.1 Hz), HH is consistently larger than HV. The smallest earthquake (M2.7), deficient in low-frequency energy, reduces the average HH for frequencies less than 1.2 Hz, but is consistent with the HH of the larger earthquakes for higher frequencies. For all frequencies, HH varies more than HV. Furthermore, the relatively narrow predominant response peak in the upper 30 m for both HH and HV (i.e., approximately 1.8 Hz) does not fully characterize the complete high-frequency amplification from the entire sediment column, which occurs over a much broader frequency range (up to approximately 7 Hz) for comparable and greater amplifications.

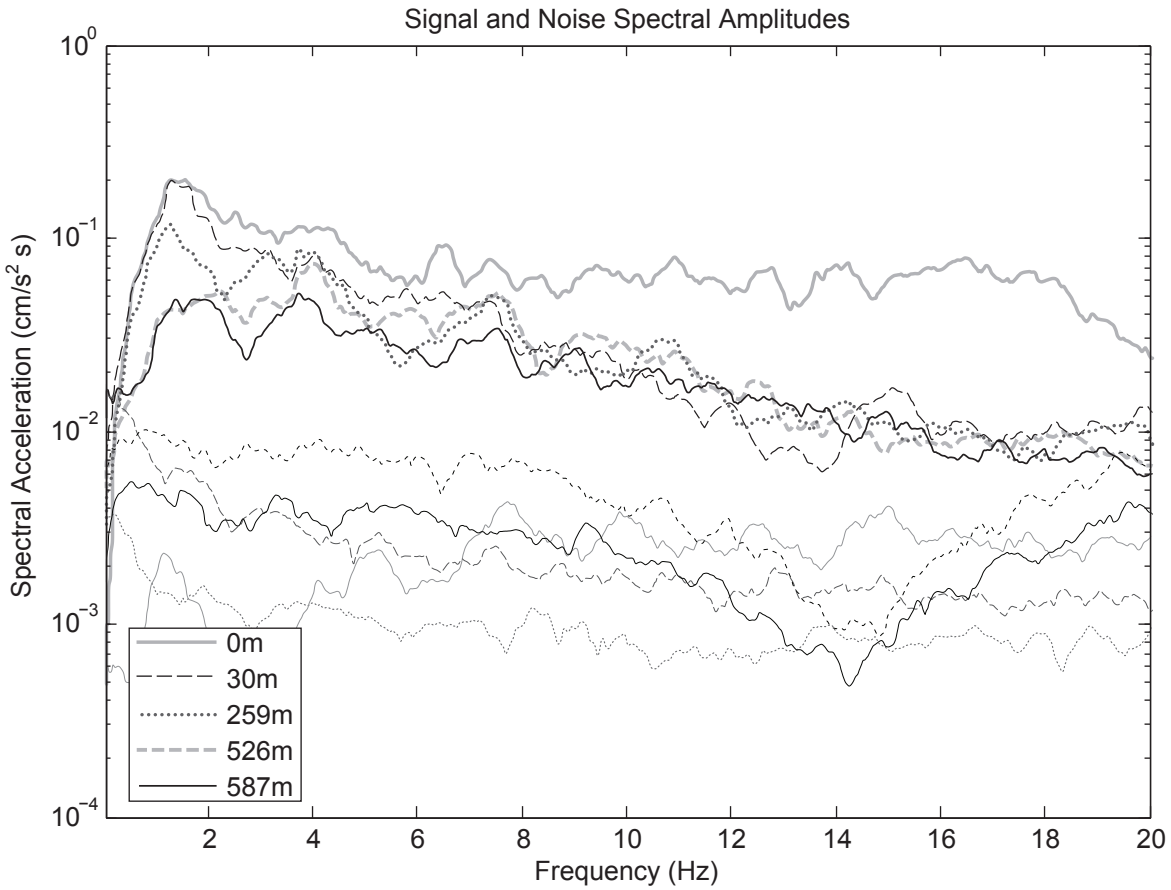

Figure 15. Acceleration amplitude spectra of the vertical-component recordings of P- and S-waves from the Feb. 28, 2011, magnitude-4.7 earthquake (upper bold lines) and pre-event noise (lower thin lines). The plotted line styles are common between the signal and noise amplitude spectra. All spectra have been smoothed with a 1-Hz running average.

Summary

The CUSSO installation has provided one of the few opportunities in the northern Mississippi Embayment to describe and measure the thick post-Paleozoic sediment using geological and geophysical methods. The installation's deepest borehole penetrated the entire 585 m of sediment overburden and terminated into the top of Late Ordovician limestone. The complex stratigraphy consists of Late Cretaceous through Holocene sands, clays, silts, and gravels, which are represented by a seven-layer intrasediment velocity model constructed using data from downhole suspension-velocity logs, surface seismic-reflection and -refraction surveys, and observed seismic-wave propagation across the vertical seismic array. The S- and P-wave velocities for the sediment range between 160 and 875 m/s, and 1,000 and 2,300 m/s, respectively. The interpreted velocity model correlates well with velocities derived from local and regional seismic-reflection and -refraction surveys (Woolery and Wang, 2012; Woolery and Almayahi, 2014). Observed time differences for S- and P-wave propagation between the bedrock and surface sensors show bulk average velocities of 610 and 1,836 m/s, respectively. The S- and P-wave bedrock velocities measured by the suspension logs are 1,452 and 3,775 m/s, respectively. The site geology is complicated by a prominent northeast-oriented fault zone beneath the array. This structure has been interpreted as a Quaternary fault, potentially representing the 34-km extension of the southern Axial Fault across the New Madrid Seismic Zone's left stepover arm (Woolery and Almayahi, 2014). Corroboration of this hypothesis would be a significant breakthrough in the intraplate seismotectonics, resolving the longstanding unbalanced strain

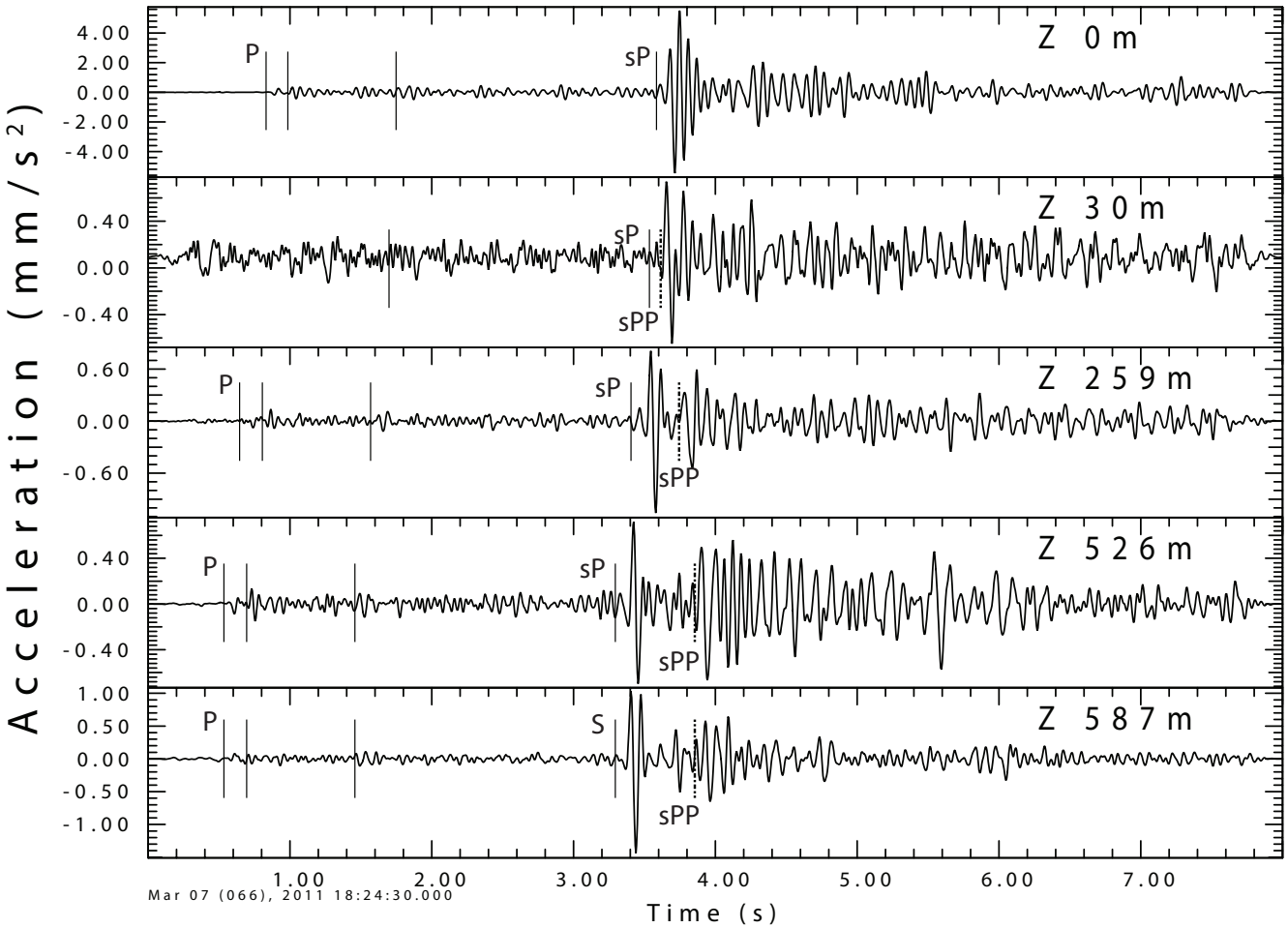

Figure 16. Vertical-component recordings, scaled individually by trace, of an M 2.3 earthquake 22 km west of CUSSO. Waveforms are instrument-corrected and bandpass-filtered from 3 to 20 Hz. P-phase, sP (upgoing S-to-P conversion), and sPP arrivals (descending sP phase reflected from the free surface) are shown with a vertical line (dashed for sPP phase) and labeled with the corresponding phase. Other upgoing P-wave arrivals are indicated with unlabeled vertical lines. Additional up- and downgoing P and sP reflections are less clear, but visible in these waveforms.

accommodation models for the New Madrid Seismic Zone.

CUSSO has recorded, despite operational difficulties, high-quality earthquake waveforms that provide insight into seismic-wave propagation in the thick Mississippi Embayment sediments, including alterations in the resultant waveform amplitude, frequency content, and duration. These alterations result from nonuniform transfer functions through the sediment overburden; different frequencies are amplified or deamplified in different intervals (Fig. 17). Although CUSSO has a limited data set for the period with operational bedrock sensors, the initial observations from the various weak-motion responses indicate that the site effect in this deep-sediment setting is not simply an effect of the shallowest layers; thus, characterization of the upper 30 m of thick sediments such as found in the Mississippi Embayment may not be accurate for larger earthquakes (e.g., compare the 0–30 m interval shown in Figure 17 with the average HH and HV curves shown in Figure 18). These observations emphasize the concerns raised by previous studies about considering V_{S30} as the sole means for evaluating site effects (see, for example, Chapman and others, 2006; Castellaro and others, 2008). In our preliminary HV measurements, the vertical and horizontal bedrock amplitudes are not equal (i.e., the average ratio in bedrock is consistently greater than unity); this assumption of unity is required for using this method for site characterization (Fig. 19).

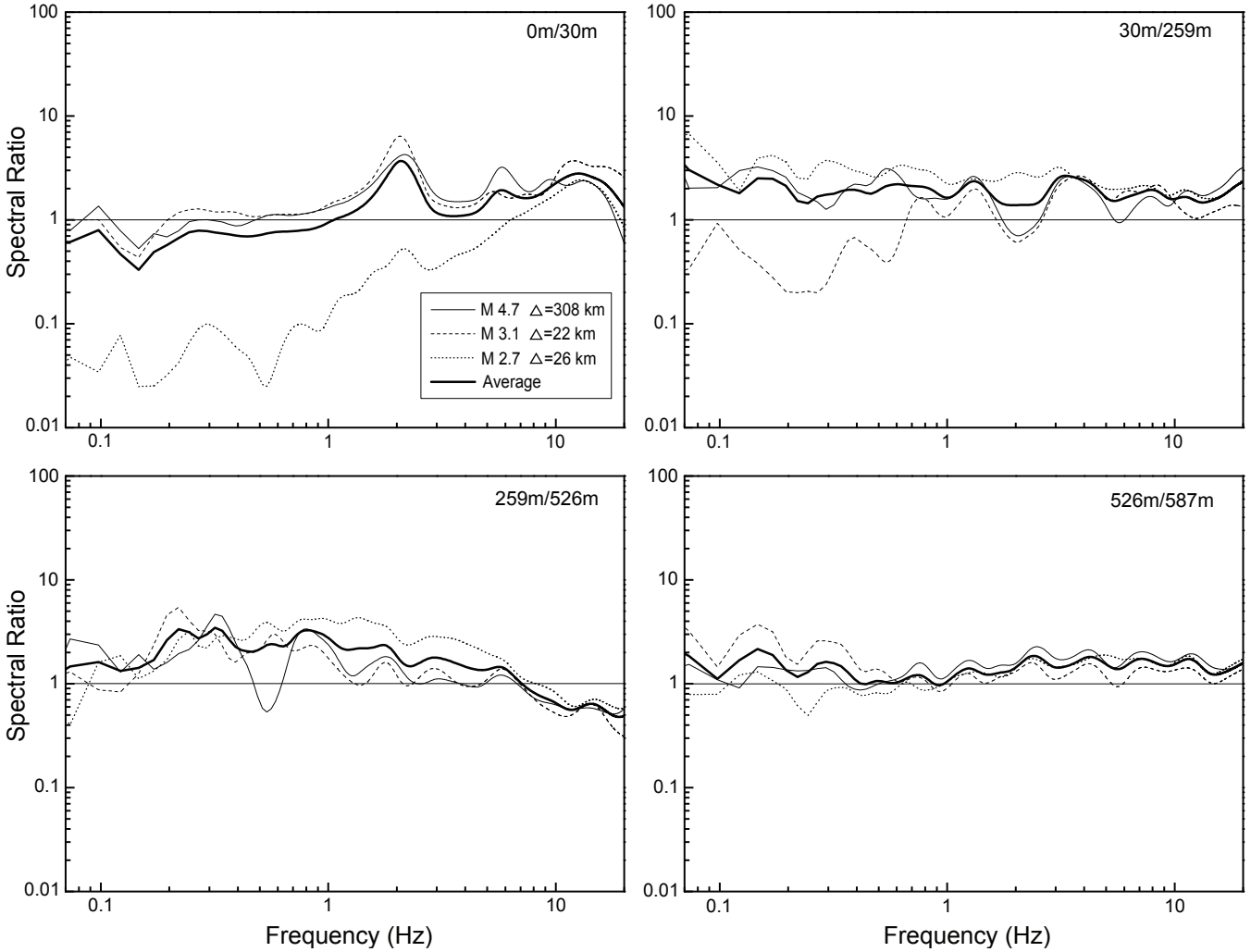

Figure 17. Spectral ratios for three earthquakes at the four sequentially instrumented intervals of the vertical array. Ratios are calculated from acceleration amplitude spectra, smoothed with a 0.5-Hz Hanning window running average. The bold, solid line in each plot is the averaged spectral ratio from the three events. The ratios suggest earthquake motions are least affected by the 526–587 m interval, but undergo a relatively broader spectral amplification and deamplification in the 259–526 m interval, at frequencies below and above 7 Hz, respectively. Amplification is more uniform in the 30–259 m interval, with the appearance of weak spectral peaks, suggesting intrainterval resonance. Dominant response peaks, corresponding with the fundamental frequency and first harmonic resonance in the upper 30 m, and overall higher frequency amplification is observed in the 0–30 m interval.

The failure of the unity assumption may be the result of the deep weathering and fracturing at the large unconformity separating the Cretaceous sediment and Ordovician limestone; additional data are needed for confirmation. Furthermore, there are noticeable differences between the spectral ratios from the directly measured transfer function (HH) and those estimated by HV (Fig. 18): The two are consistent only for a narrow band of frequencies. The effectiveness of the HV method has been evaluated by other experiments involving vertical seismic arrays, with variable results (see, for example, Theodulidis and others, 1996; Tsuboi and others, 2001; Bonilla and others, 2002). One reason for the difference between the directly observed and empirically derived transfer function is that the free surface only affects the bedrock-to-surface HH spectral ratios at high frequency; HV is insensitive to this effect because it is measured only at the surface, and the free-surface effect, experienced equally on all components, is removed by the ratio. Despite the differences, both HH and HV reveal peaks in the response at approximately 0.3 and

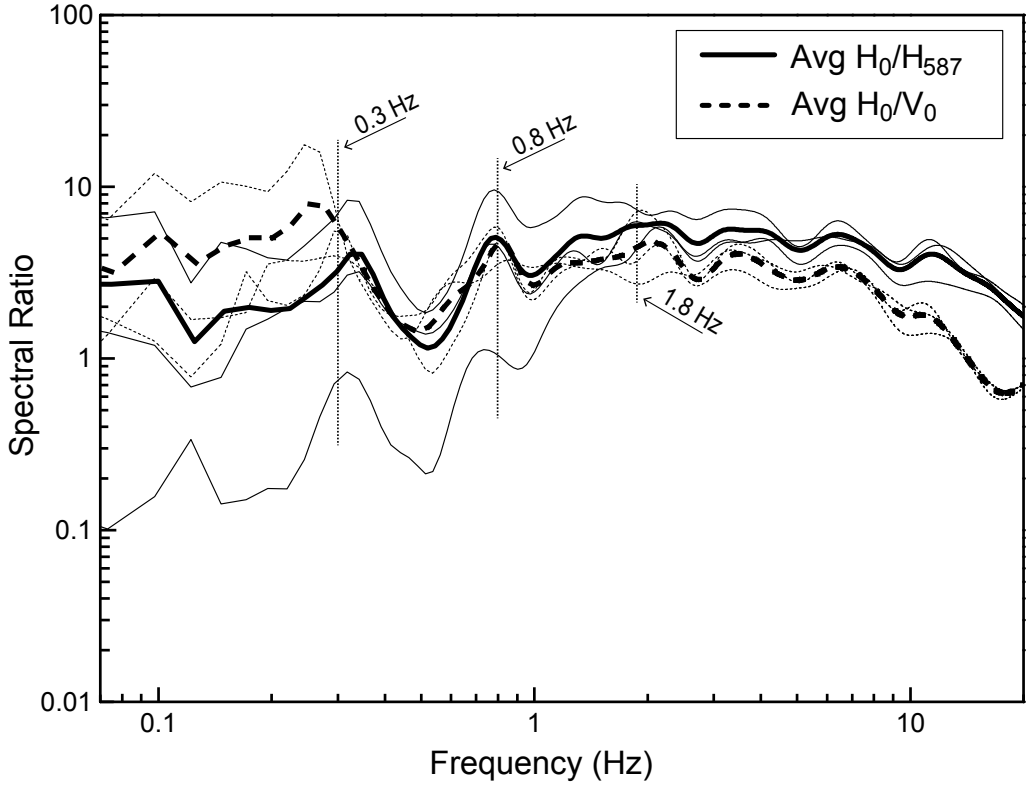

Figure 18. Average surface-to-bedrock spectral ratio (bold, solid line) and average horizontal-to-vertical spectral ratio at the surface (bold, dashed line) averaged from three earthquakes (solid and dashed thin lines, respectively). Ratios are calculated from acceleration amplitude spectra, smoothed with a 0.25-Hz window-length running average. There are notable low-frequency spectral peaks consistently at approximately 0.3 and 0.8 Hz. The frequencies at which these peaks occur are consistent with the fundamental frequency (0.26 Hz) and first harmonic (0.78 Hz) estimated for the entire sediment column. However, the average spectral ratios are only consistent within a narrow band between 0.7 and 1.1 Hz; at lower frequencies (less than 0.7 Hz), HV consistently indicates greater amplification than HH, whereas at higher frequencies (greater than 1.1 Hz), HH is consistently larger than HV. The predominant peak in the upper 30-m response (1.8 Hz; Fig. 11), does not characterize the broader range of frequencies that undergo comparable or greater levels of amplification.

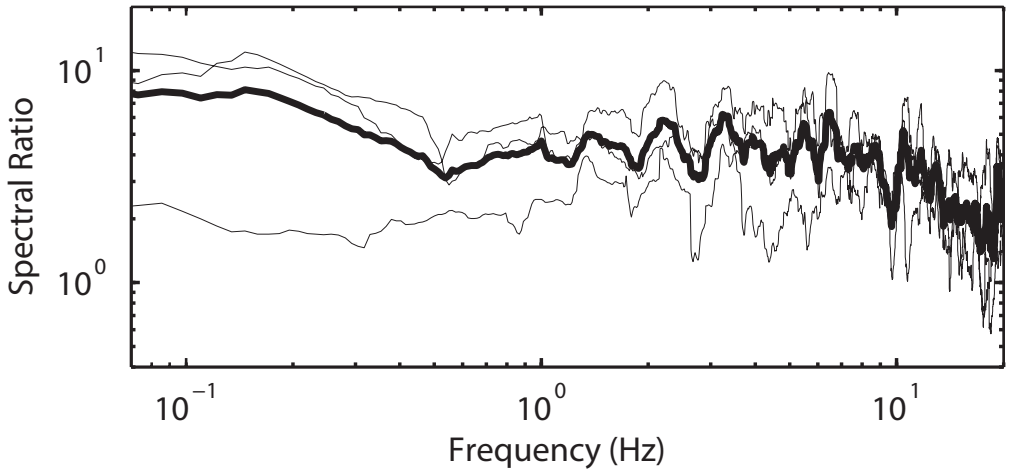

Figure 19. Horizontal-to-vertical spectral ratios of the bedrock seismometer recordings for the three earthquakes used in Figures 11 and 12 (thin lines) and their average (thick line). Ratios are calculated from acceleration amplitude spectra and smoothed with a 0.5-Hz window-length running average. With the exception of frequencies higher than 15 Hz, horizontal amplitudes are consistently greater than vertical amplitudes.

0.8 Hz as a result of shear-wave resonance within the sediment column.

Upgoing and downgoing phase arrivals (Fig. 16) can be used for basic exploration of resonance, pulse modification (e.g., broadening), and of site velocity to be determined by various methodologies; however, the full array must be operational for more earthquakes, particularly the infrequent strong-motion events, to be recorded. Observations across a broader range of magnitudes (source effects) and epicentral distances/bearings (path effects) will provide a larger set of amplitude spectra and spectral ratios from the sensors at the different depths, thus providing statistically significant constraint for the various methodologies to quantify the site effect, as well as improve calibration for the free-field seismic stations in the regional networks. To do this, CUSSO will be upgraded with instrumental hardware that is more environmentally resilient to the existing elevated hydrostatic conditions. In addition, the accelerometers deployed during this study have been found to exhibit a hysteresis response for weak, long-period signals (Greg Steiner, VLF Designs Inc., 2013, personal communication). Although outside the range of engineering interest, this behavior results in a nonlinear and unpredictable response to low-level, long-period excitations, and diminishes the data's usefulness for complete seismological applications. Nevertheless, the existing CUSSO data are useful for most purposes, and are available to interested researchers; but care must be taken to avoid incorporating undesirable noise, including degraded signal from a failing component, in any analysis. Refer to Figure 12 for guidance in selecting records from periods when sensors at the desired depths were operating properly.

Data and Resources

All data presented in this study are part of the Kentucky Seismic and Strong-Motion Network database. The high-resolution seismic-reflection data were collected and processed by faculty and students at the University of Kentucky. Unprocessed and processed versions are available from the authors. The seismic signal was processed with VISTA13 by Schlumberger-GEDCO. Topographic information used for construction of Figure 3 was from maps downloaded from the Kentucky Geological Survey. Instrument response compilation and response plots were made at the University of Kentucky with IRIS software. All data are available for download from kgs.uky.edu/kgsweb/main.asp (last accessed April 2015).

Acknowledgments

This work was financially supported by U.S. Geological Survey–NEHRP (awards 08HQGR0094 and G11AP20156), U.S. Department of Energy/Kentucky Research Consortium for Energy and Environment (award DE-FG05-03OR23032), and the Kentucky Geological Survey. The original idea for constructing a vertical seismic array in the central New Madrid Seismic Zone was conceived by Dr. Ron Street (University of Kentucky, emeritus); without his continued assistance and encouragement, this unique field experiment could not have happened. We appreciate Jonathan McIntyre (KGS, deceased) for his effort in drilling the deepest borehole and initial instrument installation. We also appreciate Steve Martin and Steve Greb (KGS) for their help with the stratigraphic interpretation and review, as well as Daniel Hunter, Shoba (Gowda) Dickinson, Anthony Paschall, David Butler, Carrington Wright, Clayton Brengman, and Ali Almayahi, who provided essential data acquisition and processing assistance. We also thank Mianshui Rong (KGS, visiting scholar) for his processing assistance, as well as Terry Hounshell and Collie Rulo (KGS) for their graphic design.

We also greatly appreciate Austin Voorhees and his family for allowing us to locate CUSSO on their property at Sassafras Ridge, Ky., and providing the University of Kentucky with a long-term right-of-entry agreement.

Various parts of this manuscript have been reviewed by Martin Chapman, Randy Cox, Jack Odum, and Roy Van Arsdale; the completed manuscript was reviewed by William Andrews and John Hickman (KGS). All the reviewers improved the manuscript considerably with their insightful comments and suggestions.

References Cited

Anderson, J.G., Lee, Y., Zeng, Y., and Day, S., 1996, Control of strong motion by the upper 30 meters: Bulletin of the Seismological Society of America, v. 86, p. 1749–1759.

Archuleta, R.J., Seale, S.H., Sangas, P.V., Baker, L.M., and Swain, S.T., 1992, Garner Valley downhole array of accelerometers: Instrumentation and preliminary data analysis: Bulletin of the Seismological Society of America, v. 82, p. 1592–1621.

Bard, P.-Y., and Chavez-Garcia, F.J., 1993, On the decoupling of surficial sediments from surrounding geology at Mexico City: Bulletin of the Seismological Society of America, v. 83, p. 1979–1991.

Bodin, P., and Horton, S., 1999, Broadband microtremor observation of basin resonance in the Mississippi Embayment, central US: Geophysical Research Letters, v. 26, p. 903–906.

Bommer, J.J., and Abrahamson, N.A., 2006, Why do modern probabilistic seismic-hazard analyses often lead to increased hazards estimates?: Bulletin of the Seismological Society of America, v. 96, p. 1967–1977.

Bonilla, L.F., Steidl, J.H., Lindley, G.T., Gariel, J.-C., and Archuleta, R.J., 2002, Borehole response studies at the Garner Valley downhole array, southern California: Bulletin of the Seismological Society of America, v. 92, p. 3165–3179.

Bonilla, M.G., 1991, The Marina District, San Francisco, California: Geology, history, and earthquake effects: Bulletin of the Seismological Society of America, v. 81, p. 1958–1979.

Bonnefoy-Claudet, S., Cotton, F., and Bard, P.-Y., 2006, The nature of noise wavefield and its applications for site effect studies. A literature review: Earth-Science Reviews, v. 79, p. 205–227.

Brengman, C., 2014, Instrument correction and dynamic site profile validation at the Central United States Seismic Observatory, New Madrid Seismic Zone: Lexington, University of Kentucky, master's thesis, 284 p.

Building Seismic Safety Council, 2009, NEHRP recommended provisions for new buildings and other structures, part I (provisions) and part II (commentary): Federal Emergency Management Agency, FEMA P-750, p. 6–8.

Castellaro, S., and Mulargia, F., 2009, The effect of velocity inversions on H/V: Pure and Applied Geophysics, v. 166, p. 567–592.

Castellaro, S., Mulargia, F., and Rossi, P.L., 2008, V_{s30}: Proxy for seismic amplification?: Seismological Research Letters, v. 79, p. 540–543.

Castro, R.R., Mucciarelli, M., Pacor, F., and Petrungaro, C., 1997, S-wave site-response estimates using horizontal-to-vertical spectral ratios: Bulletin of the Seismological Society of America, v. 87, p. 256–260.

Chapman, M.C., Martin, J.R., Olgun, C.G., and Beale, J.N., 2006, Site-response models for Charleston, South Carolina, and vicinity developed from shallow geotechnical investigations: Bulletin of the Seismological Society of America, v. 96, p. 467–489.

Chen, S.-Z., and Atkinson, G.M., 2002, Global comparisons of earthquake source spectra: Bulletin of the Seismological Society of America, v. 92, p. 885–895.

Cox, R.T., and Van Arsdale, R.B., 2002, The Mississippi Embayment, North America: A first order continental structure generated by the Cretaceous superplume mantle event: Journal of Geodynamics, v. 34, p. 163–176.

Csontos, R., and Van Arsdale, R., 2008, New Madrid Seismic Zone fault geometry: Geosphere, v. 4, p. 802–813.

Davis, R.W., Lambert, T.W., and Hansen, A.J., Jr., 1973, Subsurface geology and ground-water resources of the Jackson Purchase Region, Kentucky: U.S. Geological Survey Water-Supply Paper 1987, 66 p.

Field, E.H., Kramer, S., Elgamal, A.-W., Bray, J.D., Matasovic, N., Johnson, P.A., Cramer, C., Roblee, C., Wald, D.J., Bonilla, L.F., Dimitriu, P.P., and Anderson, J.G., 1998, Nonlinear site response: Where we're at (a report from a SCEE/PEER seminar and workshop): Seismological Research Letters, v. 69, p. 230–234.

Finch, W.I., 1971, Geologic map of the Bondurant quadrangle, Fulton County, Kentucky, and New Madrid, Mississippi County, Missouri: U.S. Geological Survey Geologic Quadrangle Map GQ-918, scale 1:24,000.

Idriss, M., and Sun, J.I., 1992, User's manual for SHAKE91: A computer program for conducting equivalent linear seismic response

analysis of horizontally layered soil deposits: University of California, Davis, Center for Geotechnical Modeling, Department of Civil and Environmental Engineering, 13 p.

Johnston, A.C., and Schweig, E.S., 1996, The enigma of the New Madrid earthquakes of 1811-1812: Annual Review of Earth and Planetary Science, v. 24, p. 339–384.

Lermo, J., and Chavez-Garcia, F.J., 1993, Site effect evaluation using spectral ratios with only one station: Bulletin of the Seismological Society of America, v. 83, p. 1574–1594.

McDowell, R.C., Grabowski, G.J., and Moore, S.L., 1981, Geologic map of Kentucky: U.S. Geological Survey, scale 1:250,000.

Molnar, S., Cassidy, J.F., and Dosso, S.E., 2004, Comparing intensity variation of the 2001 Nisqually earthquake with geology in Victoria, British Columbia: Bulletin of the Seismological Society of America, v. 94, p. 2229–2238.

Nakamura, Y., 1989, A method for dynamic characteristics estimation of subsurface using microtremor on the ground surface: Quarterly Report of Railway Technical Research Institute, v. 30, p. 25–33.

Nelson, W.J., 1998, Bedrock geology of the Paducah 1° x 2° CUSMAP quadrangle, Illinois, Indiana, Kentucky, and Missouri: U.S. Geological Survey Bulletin 2150-B, 36 p.

Odum, J., Stephenson, W., Shedlock, K., and Pratt, T., 1998, Near-surface structural model for deformation associated with the February 7, 1812, New Madrid, Missouri, earthquake: Geological Society of America Bulletin, v. 110, p. 149–162.

Olive, W.W., 1980, Geologic maps of the Jackson Purchase Region, Kentucky: U.S. Geological Survey Miscellaneous Investigations Map I-1217, scale 1:250,000.

Potter, P.E., and Pryor, W.A., 1961, Dispersal centers of Paleozoic and later clastics of the upper Mississippi Valley and adjacent areas: Geological Society of America Bulletin, v. 72, p. 1195–1249.

Pratt, T.L., 2012. Kinematics of the New Madrid Seismic Zone, central U.S., based on stepover models: Geology, v. 40, p. 371–374.

Pratt, T.L., Williams, R.A., Odum, J.K., and Stephenson, W.J., 2012, Origin of the Blytheville Arch, and long-term displacement on the New Madrid Seismic Zone, central United States, *in* Cox, R.T., Tuttle, M.P., Boyd, O.S., and Locat, J., eds., Recent advances in North American paleoseismology and neotectonics east of the Rockies: Geological Society of America Special Paper 493, p. 1–15, doi:10.1130/2012.2493(01).

Rong, M., Wang, Z., Woolery, E.W., Lyu, Y., and Li, X., 2016, Nonlinear site response from the strong ground-motion recordings in western China: Soil Dynamics and Earthquake Engineering, v. 82, p. 99–110.

Schnabel, P.B., Lysmer, J., and Seed, H.B., 1972, SHAKE: A computer program for earthquake response analysis of horizontally layered sites: University of California, Berkeley, Earthquake Engineering Research Center, Report EERC 72-12, 88 p.

Schwalb, H.R., 1969, Paleozoic geology of the Jackson Purchase Region, Kentucky: Kentucky Geological Survey, ser. 10, Report of Investigations 10, 40 p.

Seed, H.B., Romo, M.P., Sun, J.I., Jaime, A., and Lysmer, J., 1988, The Mexico earthquake of September 19, 1985—Relationships between soil conditions and earthquake ground motions: Earthquake Spectra, v. 4, p. 687–729.

Shearer, P.M., and Orcutt, J.A., 1987, Surface and near-surface effects on seismic waves—Theory and borehole seismometer results: Bulletin of the Seismological Society of America, v. 77, p. 1168–1196.

Steidl, J.H., Tumarkin, A.G., and Archuleta, R.J., 1996, What is a reference site?: Bulletin of the Seismological Society of America, v. 86, p. 1733–1748.

Theodulidis, N., Bard, P.-Y., Archuleta, R., and Bouchon, M., 1996, Horizontal-to-vertical spectral ratio and geological conditions: The case of Garner Valley downhole array in southern California: Bulletin of the Seismological Society of America, v. 86, p. 306–319.

Toro, G.R., Silva, W.J., McGuire, R.K., and Herrmann, R.B., 1992, Probabilistic seismic hazard mapping of the Mississippi Embayment: Seismological Research Letters, v. 63, p. 449–475.

Tsuboi, S., Saito, M., and Ishihara, Y., 2001, Verification of horizontal-to-vertical spectral-ratio technique for estimation of site response

using borehole seismographs: Bulletin of the Seismological Society of America, v. 91, p. 499–510.

Tuttle, M.P., Schweig, E.S., Sims, J.D., Lafferty, R.H., Wolf, L.W., and Haynes, M.L., 2002, The earthquake potential of the New Madrid Seismic Zone: Bulletin of the Seismological Society of America, v. 92, p. 2080–2089.

Van Arsdale, R.B., Kelson, K.I., and Lumsden, C.H., 1995, Northern extension of the Tennessee Reelfoot Scarp into Kentucky and Missouri: Seismological Research Letters, v. 55, p. 57–62.

Van Arsdale, R.B., and TenBrink, R.K., 2000, Late Cretaceous and Cenozoic geology of the New Madrid Seismic Zone: Bulletin of the Seismological Society of America, v. 90, p. 345–356.

Wald, L.A., and Mori, J., 2000, Evaluation of methods for estimating linear site-response amplifications in the Los Angeles region: Bulletin of the Seismological Society of America, v. 90, no. 6B, p. S32–S42.

Woolery, E., and Almayahi, A., 2014, Northeast-oriented transpression structure in the northern New Madrid Seismic Zone—Extension of a shear zone across the Reelfoot fault stepover arm: Bulletin of the Seismological Society of America, v. 104, p. 2587–2596.

Woolery, E., and Wang, Z., 2010, Toward construction of the Central United States Seismic Observatory and calibration site: Defining the geologic site model: U.S. Geological Survey National Earthquake Hazards Reduction Program Final Technical Report 08HQGR0094, 33 p.

Woolery, E., and Wang, Z., 2012, Toward construction of the Central United States Seismic Observatory and calibration site: Defining the geologic site model, part 2: U.S. Geological Survey National Earthquake Hazards Reduction Program Final Technical Report G11AP20156, 32 p.